

## TOWARD AROA INHIBITOR DESIGN

**TRANSITION STATE ANALYSIS OF THE AROA REACTION USING KINETIC  
ISOTOPE EFFECTS**

**By**

**MEIYAN LOU, B. Sc.**

**A Thesis**

**Submitted to the School of Graduate Studies**

**in Partial Fulfillment of the Requirements**

**for the Degree**

**Master of Science**

**McMaster University**

**© Copyright by Meiyang Lou, September 2008**

**MASTER OF SCIENCE (2008)**

**McMaster University**

**(Biochemistry and Biomedical Sciences)**

**Hamilton, Ontario**

**TITLE:           Transition State Analysis of the AroA Reaction Using Kinetic  
Isotope Effects**

**AUTHOR:        Meiyan Lou, B. Sc. (Peking University, Beijing, P. R. China)**

**SUPERVISOR:    Dr. Paul J. Berti**

**NUMBER OF PAGES: xi, 73**

## **Abstract**

AroA catalyzes the sixth step of the shikimate biosynthetic pathway which produces aromatic amino acids in plants and bacteria, but is absent in mammals. This makes AroA an attractive antimicrobial target. The transition state (TS) structures of AroA- and acid-catalyzed 5-*enol*pyruvyl shikimate-3-phosphate (EPSP) hydrolysis were studied in atomic detail by kinetic isotope effect (KIE) measurement. Enzymes bind their transition states more tightly than any other species, so molecules that closely resemble the transition state would have a high affinity for the enzyme and be good inhibitors. Radiolabelled EPSPs were synthesized and a KIE measurement method was developed. Six KIEs were measured for both the AroA- and acid-catalyzed reactions. KIEs for the AroA reaction indicate a cationic TS structure. The acid-catalyzed reaction may employ a slightly different mechanism with an earlier TS. A computational TS model was found and its KIEs were calculated. It demonstrated good agreement with the experimental values at most positions. The model is being modified to improve the agreement with the experimental KIEs. This TS structure will be a good starting point for inhibitor design. All these efforts, hopefully, can make a positive contribution to the development of antimicrobial drugs.

## **Acknowledgements**

I would like to thank my supervisor Dr. Paul Berti for giving me this opportunity to come to McMaster University and work on this project. Thank you for all your valuable guidance and instructions, and especially your patience and encouragement in face of ups and downs throughout the project. To my committee members, Dr. Eric Brown and Dr. Giuseppe Melacini, thank you for your feedback and suggestion along the three committee meetings. As well, I would like to thank Dr. Kirk Green and Dr. Jiaxi Wang for their assistance in mass spectrometry.

I would also like to thank Paul Chindemi, Amanda Ramnarine, Mohamed Chagalov, Ed Morrison, Vivian Gawuga, Naresh Balachandran and other Berti lab members, for your generous advice and great help during these two years. You create a fantastic lab environment. This two-year journey with you is a sweet memory for me for ever.

To all my friends in biochemistry, chemistry and chemical engineering, I am so lucky to have loyal and lovely people like you around me. Thank you for accompanying and helping me all along the way.

Finally, I want to thank my parents, away in China, for your unending love and constant support for 25 years. I would not have gone that far without your encouragement. Thank you for everything you have done for me.

## **Table of Contents**

Abstract.....	iii
Acknowledgements .....	iv
Table of Contents .....	v
List of Abbreviations .....	vii
List of Figures.....	ix
List of Tables .....	xi
Introduction .....	1
Enzyme of interest - AroA .....	2
Reaction catalyzed by AroA. ....	2
Proposed mechanism of AroA reaction .....	3
An important side product - EPSP ketal .....	6
X-ray crystal structures.....	7
Controversy over the identity of catalytic residues .....	9
Alternative reactions.....	11
Inhibitors of AroA reaction .....	12
Transition state theory.....	14
Transition state and kinetic isotope effect (KIE) .....	15
The sources of KIEs.....	17
Methods to measure KIEs.....	19
Remote labels for KIE measurement by radioactivity.....	20
Computational EIEs/KIEs.....	22
Objective of this project.....	24
Methods .....	25
General .....	25
Protein purification .....	25

Characterization of purified AroA.....	26
EPSP synthesis and hydrolysis.....	27
SDKIE of AroA-catalyzed EPSP hydrolysis.....	28
Synthesis of radiolabelled EPSPs.....	29
KIE measurement for AroA-catalyzed EPSP hydrolysis.....	32
KIE measurement for acid-catalyzed EPSP hydrolysis.....	33
Testing KIE measurement method.....	34
Computational EIE/KIE calculation.....	35
<b>Results.....</b>	<b>37</b>
AroA purification.....	37
SDKIE of AroA-catalyzed EPSP hydrolysis.....	38
Synthesis of radiolabelled EPSPs.....	39
Optimization of KIE measurement conditions.....	43
Remote labels.....	46
KIEs from AroA-catalyzed EPSP hydrolysis.....	47
KIEs from acid-catalyzed EPSP hydrolysis.....	49
Computational TS structures and their corresponding EIE/KIE.....	53
<b>Discussion.....</b>	<b>56</b>
Kinetically significant steps.....	56
SDKIE from AroA-catalyzed EPSP hydrolysis.....	57
Method development.....	57
Interpretation of KIEs from AroA-catalyzed EPSP hydrolysis.....	58
Interpretation of KIEs from acid-catalyzed EPSP hydrolysis.....	62
Computational TS and experimental TS.....	66
<b>Conclusions and Future Work.....</b>	<b>69</b>
<b>References.....</b>	<b>70</b>

## **List of Abbreviations**

<b>AroA:</b>	<b>5-<i>enol</i>pyruvyl shikimate 3-phosphate synthase</b>
<b>AroK:</b>	<b>shikimate kinase</b>
<b>ddS3P:</b>	<b>4,5-dideoxyshikimate 3-phosphate</b>
<b>EIE:</b>	<b>equilibrium isotope effect</b>
<b>EPSP:</b>	<b>5-<i>enol</i>pyruvyl shikimate-3-phosphate</b>
<b>EXC:</b>	<b>excited state energy</b>
<b>G6PDH:</b>	<b>glucose 6-phosphate dehydrogenase</b>
<b>IPTG:</b>	<b>isopropyl-<math>\beta</math>-D-thiogalactopyranoside</b>
<b>KIE:</b>	<b>kinetic isotope effect</b>
<b>MG/AM:</b>	<b>Malachite Green / ammonium molybdate</b>
<b>MMI:</b>	<b>mass and moment of inertia</b>
<b>MurA:</b>	<b>UDP-<i>N</i>-acetylglucosamine <i>enol</i>pyruvyl transferase</b>
<b>PEP:</b>	<b>phospho<i>enol</i>pyruvate</b>
<b>PGM:</b>	<b>phosphoglucomutase</b>
<b>Pi:</b>	<b>inorganic phosphate</b>
<b>PMSF:</b>	<b>phenylmethylsulfonyl fluoride</b>
<b>ppsA:</b>	<b>phospho<i>enol</i>pyruvate synthetase</b>

<b>S3P:</b>	<b>shikimate 3-phosphate</b>
<b>SCRF:</b>	<b>self consistent reaction field</b>
<b>SP:</b>	<b>sucrose phosphorylase</b>
<b>SDKIE:</b>	<b>solvent deuterium kinetic isotope effect</b>
<b>TBAS:</b>	<b>tetrabutylammonium sulfate</b>
<b>THI:</b>	<b>tetrahedral intermediate</b>
<b>TS:</b>	<b>transition state</b>
<b>ZPE:</b>	<b>zero point energy</b>

## List of Figures

Figure 1. AroA catalyzes the reaction from PEP and S3P to EPSP and Pi. ....	2
Figure 2. Two-step pathway of AroA reaction. ....	3
Figure 3. Equilibrium among THI, cation, EPSP and the formation of EPSP ketal.	7
Figure 4. Crystal structures of AroA. ....	8
Figure 5. Different general acid/base candidates proposed as catalytic residues.	9
Figure 6. AroA and acid catalyzed EPSP hydrolysis to S3P and pyruvate. ....	11
Figure 7. EPSP cation as the common species for three pathways. ....	12
Figure 8. Structures related to glyphosate. ....	13
Figure 9. Normal and inverse KIEs. ....	18
Figure 10. $E_{\max}$ of the $\beta$ -particle from $^{14}\text{C}$ and $^{32}\text{P}$ . ....	21
Figure 11. Computational structures for KIE/EIE calculation. ....	35
Figure 12. Fluorescence titration for AroA active concentration. ....	37
Figure 13. MG/AM assay for AroA activity. ....	38
Figure 14. Rates of S3P production in one individual trial. ....	39
Figure 15. Radiolabelled EPSPs for KIE measurement. ....	40
Figure 16. $[1',1'\text{-}^{18}\text{O}_2]\text{EPSP}$ synthesis. ....	41
Figure 17. $[5\text{-}^{18}\text{O}]\text{EPSP}$ synthesis. ....	42
Figure 18. $[3',3'\text{-}^2\text{H}_2]\text{EPSP}$ synthesis. ....	43
Figure 19. Energy profiles of $^{14}\text{C}$ versus $^{32}\text{P}$ and $^{33}\text{P}$ versus $^{32}\text{P}$ . ....	44
Figure 20. Radioactivity distribution of EPSP hydrolysis, ....	45
Figure 21. Summary of KIEs for AroA-catalyzed EPEP hydrolysis. ....	49
Figure 22. KIEs for acid-catalyzed EPEP hydrolysis. ....	52
Figure 23. TS model with one guanidinium ion and three water molecules. ....	54
Figure 24. Kinetically significant steps in the reaction coordinate. ....	56
Figure 25. Reaction diagram for possible mechanisms of addition steps of EPSP hydrolysis. ....	59
Figure 26. Proposed TS structures for acid catalyzed hydrolysis. ....	63
Figure 27. Comparison of calculated EIEs/KIEs with the experimental KIEs for	

AroA-catalyzed hydrolysis. ....	66
Figure 28. Comparison of calculated EIEs/KIEs with the experimental KIEs for acid-catalyzed hydrolysis.....	67

## List of Tables

Table 1. SDKIE for AroA-catalyzed EPSP hydrolysis .....	39
Table 2. Radiolabelled EPSPs synthesized for KIE measurement.....	40
Table 3. Isotope ratios before and after HPLC separation.....	46
Table 4. $^{32}\text{P}/^{33}\text{P}$ KIE for AroA-catalyzed EPSP hydrolysis .....	47
Table 5. $[1'-^{14}\text{C}]$ EPSP KIE for AroA-catalyzed hydrolysis .....	47
Table 6. $[2'-^{14}\text{C}]$ EPSP KIE for AroA-catalyzed hydrolysis .....	47
Table 7. $[3'-^{14}\text{C}]$ EPSP KIE for AroA-catalyzed hydrolysis .....	48
Table 8. $[3',3'-^2\text{H}_2]$ EPSP KIE for AroA-catalyzed hydrolysis .....	48
Table 9. $[5-^{18}\text{O}]$ EPSP KIE for AroA-catalyzed hydrolysis.....	48
Table 10. $[1',1'-^{18}\text{C}_2]$ EPSP KIE for AroA-catalyzed hydrolysis.....	48
Table 11. $[1'-^{14}\text{C}]$ EPSP KIE for acid-catalyzed hydrolysis.....	50
Table 12. $[2'-^{14}\text{C}]$ EPSP KIE for acid-catalyzed hydrolysis .....	50
Table 13. $[3'-^{14}\text{C}]$ EPSP KIE for acid-catalyzed hydrolysis .....	50
Table 14 $[3',3'-^2\text{H}_2]$ EPSP KIE for acid-catalyzed hydrolysis .....	51
Table 15. $[5-^{18}\text{O}]$ EPSP KIE for acid-catalyzed hydrolysis.....	51
Table 16. $[1',1'-^{18}\text{C}_2]$ EPSP KIE for acid-catalyzed hydrolysis .....	52
Table 17. Calculated EIEs/KIEs for AroA-catalyzed hydrolysis at 310 K .....	55
Table 18. Calculated EIEs/KIEs for acid-catalyzed hydrolysis at 363 K .....	55

## **Introduction**

The discovery of antibiotics is a milestone in humankind's history to fight against diseases and deaths caused by infectious microorganisms. However, drug resistance has emerged and increased rapidly during the last few decades (1). We are faced with pan-resistant bacteria - bacteria resistant to all existing antibiotics. As a result, there is a constant demand for the study of antibiotic resistance and the development of new antimicrobial drugs.

Enzymes are important targets in antibiotic design due to their essential role in organisms. A large number of enzyme inhibitors resemble the substrates, intermediates or more recently, the transition state (TS) of enzymes (2). Rather than substrates or products, enzymes have the highest affinity for the TS structures (3). It should be difficult, therefore, if not impossible, for an enzyme to avoid binding a sufficiently good TS mimic while retaining catalytic activity. This will help prevent the development of resistance.

The enzyme AroA (*5-enolpyruvyl shikimate 3-phosphate synthase*) and its mechanism are the focus of my project. AroA is an essential enzyme to produce aromatic amino acids through the shikimate pathway in plants and bacteria (4), but absent in mammals, making it an attractive target for antibiotic design (5). Due to its unusual chemistry and its potential value in antimicrobial research, AroA has been the subject of numerous studies since 1980s (6-8). This thesis describes the current progress in exploring the transition state structure of AroA's reaction in

order to cast light on effective inhibitor design and enzymatic mechanism investigation.

### Enzyme of interest - AroA

AroA is one of only two enzymes known to catalyze carboxyvinyl transfer. The other is UDP-*N*-acetylglucosamine *enol*pyruvyl transferase (MurA) in the peptidoglycan synthesis pathway. AroA catalyzes the reaction from phospho*enol*pyruvate (PEP) and shikimate 3-phosphate (S3P) to form 5-*enol*pyruvyl shikimate-3-phosphate (EPSP) and inorganic phosphate (Pi) (Figure 1) (6), the sixth step of shikimate biosynthetic pathway (4). The plant homologue of AroA is inhibited by glyphosate (*N*-(phosphonomethyl)glycine), the active ingredient in the herbicide Roundup (7). Although it is an effective herbicide, glyphosate is not an antibiotic, probably because its anionic phosphonate group prevents it from penetrating the cell walls. Great efforts are being taken to find potent inhibitors of AroA which could act as an antibiotic.

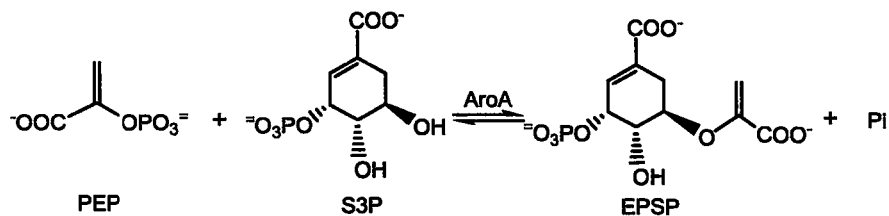
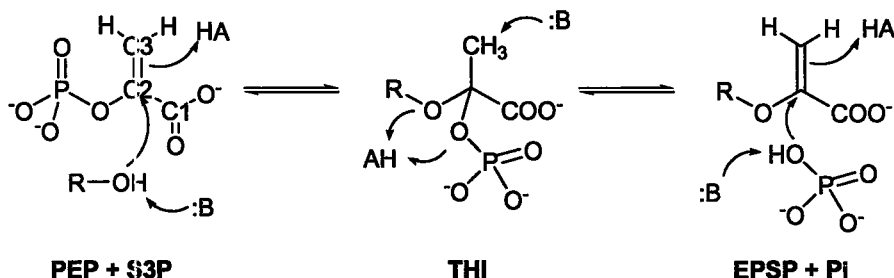


Figure 1. AroA catalyzes the reaction from PEP and S3P to EPSP and Pi.

### Reaction catalyzed by AroA.

AroA catalyzes a fully reversible reaction, with equilibrium favouring the forward direction by 15-fold (6). This reaction proceeds via an addition-elimination

pathway through a non-covalent tetrahedral intermediate (THI) (9). During the addition step, the C3 of PEP is protonated by a general acid and the C2 is attacked by 5-OH of S3P, giving rise to THI. In the elimination step, the phosphate group leaves and C3' is deprotonated by a general base, re-forming the double bond between C2' and C3' (Figure 2) (10). This is essentially the reverse of the addition step, but with phosphate as the leaving group.



**Figure 2. Two-step pathway of AroA reaction.** R-OH: S3P; HA, :B: general acid/base. (ref. 10)

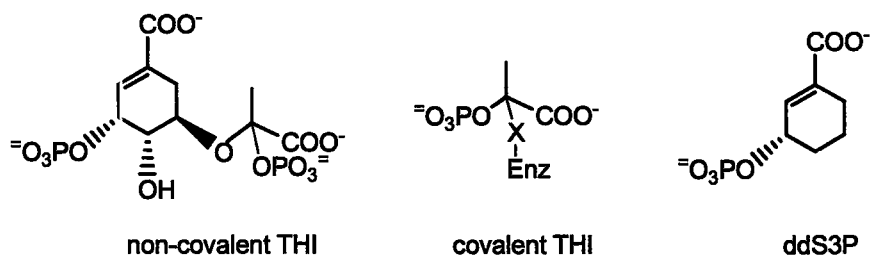
### Proposed mechanism of AroA reaction

The reaction pathway and kinetic mechanism of AroA have been well investigated and most of its kinetic parameters have been determined (6). However, there are still several aspects of the reaction that are not well understood, and require more further investigation.

AroA's reaction was first proposed to be ordered, with S3P binding first, followed by PEP, then EPSP being released first, followed by Pi. This was supported by the fact that glyphosate is a competitive inhibitor of PEP but uncompetitive with respect to S3P (11). Moreover, recent crystal structures from *S. pneumoniae* AroA indicated that the residues involved in S3P binding are located

in the N-terminal domain while residues for PEP or glyphosate binding are evenly distributed in both N-terminal and C-terminal domains (12). It implies that S3P can bind enzyme in an open conformation while the binding of PEP or glyphosate can only occur after the two domains move together into a closed conformation (12). However, further steady-state kinetic results demonstrated that both the forward (13) and reverse reactions (14) are random with synergistic binding of substrates, with competitive inhibition being observed between substrates.

The formation of a non-covalent THI in the AroA reaction has been widely accepted. However, it was once believed that AroA acted as the nucleophile to form a covalently-bound intermediate. This assumption was mainly based on certain  $^{13}\text{C}$  NMR observations (15) as well as the experimental fact that AroA catalyzes the exchange of solvent  $^3\text{H}$  into C3 of PEP in the presence of 4,5-dideoxyshikimate 3-phosphate (ddS3P) (11). Other evidence supporting a covalently-bound intermediate came from MurA, which was also believed at that time to employ a covalent intermediate (16).



However, Jakeman et al. in 1998 argued that the compound observed by NMR was simply EPSP ketal, a side product of AroA reaction (17). Moreover, the solvent  $^3\text{H}$  exchange could be explained by the formation of PEP cation. More

importantly, with the development of rapid chemical quench methodology, single turnover experiments were performed on a millisecond timescale. A non-covalent THI was successfully trapped and its identity confirmed by HPLC and NMR (18). THI is stable enough in the basic environment to be purified and studied in detail. At pH 7, it has a half-life of 15 min; while when the pH increases to above 12, its half-life is 24 days (19). It was further determined that in the presence of AroA, THI broke down within 50 ms and partitioned in the forward and reverse directions, consistent with AroA's steady-state turnover rate, demonstrating that THI is kinetically competent (20). Since then, the status of THI as a non-covalent intermediate of AroA reaction has been overwhelmingly established.

A non-covalent THI was also isolated and characterized from MurA (21). However, MurA has a covalent THI as well, although it is not catalytically relevant (18).

The reaction stereochemistry is another important question. It has been confirmed that the addition and elimination steps of AroA reaction proceed with opposite stereochemistry (22). If addition is *anti*, then the elimination step will have to be *syn*, or vice versa. The addition of proton at C-3 of PEP was demonstrated to be on the *si* face by using (E)- and (Z)-fluoro-PEP running reactions in D<sub>2</sub>O, and analysing their corresponding THI configuration (23). Further evidence illustrated that THI employed an *S*-configuration while the *R*-THI was inert to AroA, supporting an *anti* addition (24). Taking all the stereochemical information together, it was accepted that AroA's reaction proceeds with *anti*

addition and *syn* elimination (24). Eschenburg et al. later proposed the reverse configuration, that is, *syn* addition and *anti* elimination, because the side chain that they proposed to deprotonate C3' in the elimination step and the leaving group (Pi) were on the opposite faces of PEP based on their mutant AroA structures (25).

### **An important side product - EPSP ketal**

Concurrently with the discovery of the intermediate, EPSP ketal, a side product of the AroA reaction was discovered and isolated after extended incubation with the enzyme (17). EPSP ketal was originally assumed to derive from non-enzymatic breakdown of THI which had dissociated from AroA's active site (26). However, our laboratory was able to demonstrate that EPSP ketal is synthesized in the enzyme's active site in the presence of excess AroA, though the formation is too slow for it to be a catalytic intermediate (27). The formation of EPSP ketal is convincing evidence for a cationic intermediate. EPSP ketal is produced through intramolecular nucleophilic attack by 4-OH of S3P on C2'. In the normal reverse reaction, AroA activates phosphate as a nucleophile to attack C2'; however, 4-OH is a poor nucleophile and located on the opposite side of C2' from Pi. Since C2' is not subject to nucleophilic attack in its *eno*/pyruvyl form, it is reasonable to presume the existence of a highly cationic intermediate, which would make the nucleophilic attack from 4-OH possible (Figure 3) (27).

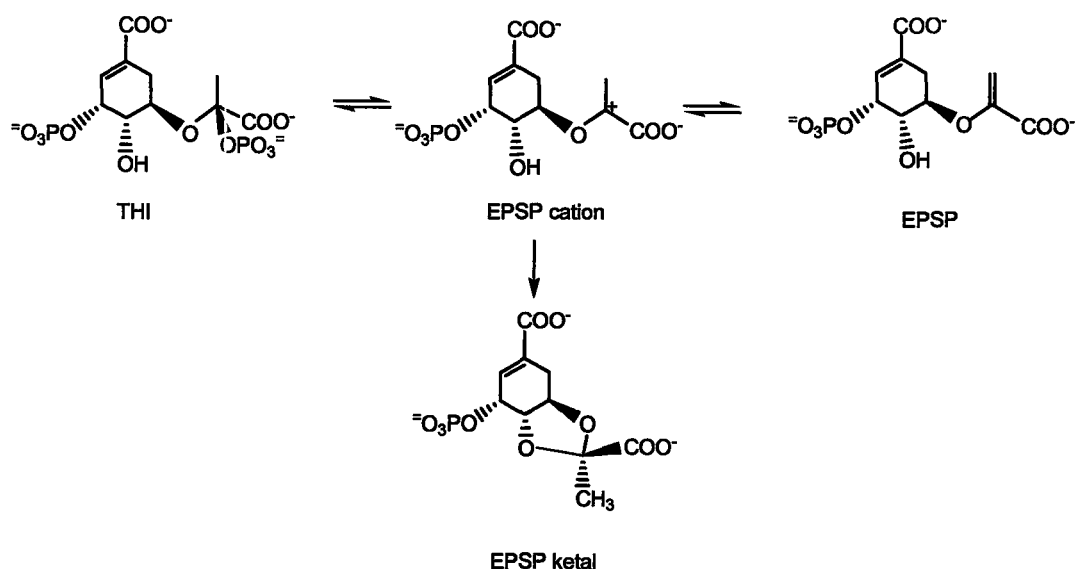


**Figure 3. Equilibrium among THI, cation, EPSP and the formation of EPSP ketal. (ref. 27)**

### X-ray crystal structures

AroA is a 46 kDa, 462 amino acid protein comprised of a single polypeptide chain (17). The X-ray crystal structure of *E. coli* AroA at 3.0 Å resolution showed a distinctive fold containing two similar domains, which are connected by two peptide crossovers (28). Each domain is made up of three repetitive folding units comprising two  $\alpha$ -helices and four  $\beta$ -strands, in a  $\beta\alpha\beta\alpha\beta\beta$ -pattern (28). The crystal structure of substrate-free MurA has also been determined at 2.0 Å resolution, revealing a similar overall fold to AroA (29), in spite of only 25% sequence identity (6). MurA and AroA are the only two enzymes found to have this characteristic fold (29).

Crystal structures of AroA complexed with S3P, and with both S3P and glyphosate at resolutions of 1.6 Å and 1.5 Å respectively, were also solved (8). With the substrate and inhibitor bound, the two domains of AroA were in a closed

conformation, forming the active site at the interface (Figure 4) (8). The approach of the two domains to form a closed conformation upon binding of substrate and inhibitor is the basis of the fluorescence titration described in the Method section. Those crystal structures provide insight in future studies of AroA, including functional assignment of amino acid residues, glyphosate's inhibitory mode and potential inhibitor screening.

More recently, the crystal structures of AroA from *Streptococcus pneumoniae*, in an unliganded state, complexed with fluoro-tetrahydro intermediate, as well as S3P-glyphosate bound state, were also reported at resolutions from 2.3 Å to 1.9 Å (12). The structures are similar to those of *E.coli* AroA with slight differences in topology (12).

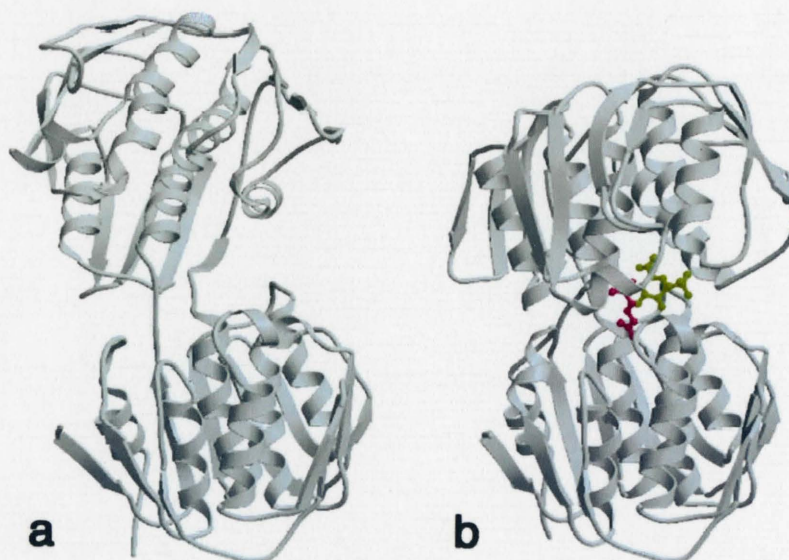


**Figure 4. Crystal structures of AroA.** a). Free AroA structure in an open conformation; b). AroA in a closed conformation with S3P and glyphosate bound, shown as ball-and-stick models in yellow and magenta, respectively. (ref. 8)

## Controversy over the identity of catalytic residues

Identification of the key catalytic residues for the AroA reaction has been controversial. It is widely accepted that the addition and elimination steps employ opposite stereochemistry, but different groups suggested different candidates as catalytic residues (Figure 5).

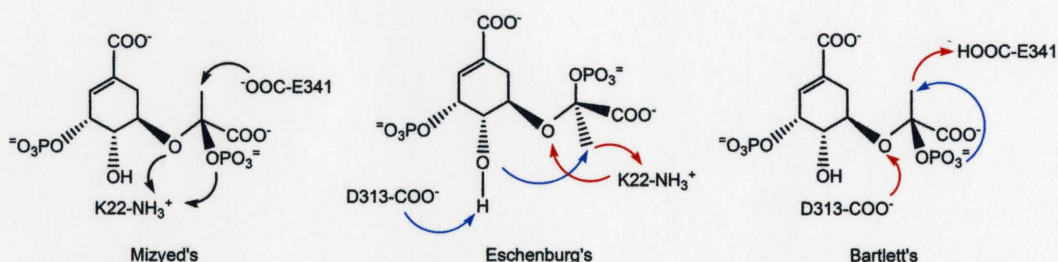


**Figure 5. Different general acid/base candidates proposed as catalytic residues.** All the interactions are shown in THI form. Red arrows stand for interactions in the addition step, blue arrows for the elimination step, and black arrows for both steps.

Shehadeh Mizyed from our group proposed that THI breakdown forward to products or backward to reactants used the same general acid/base catalytic pair, Lys22 and Glu341 (30). In the addition step, Glu341 acted as the general acid to protonate C3 of PEP, and Lys22 was the general base to deprotonate 5-OH of S3P. Conversely, during the elimination step, Glu341 served as the general base to deprotonate C3' of the THI, and Lys22 acted as the general acid to protonate the leaving group, either S3P or phosphate (30). This was based on the experimental observation that none of the single amino acid mutants of AroA significantly changed THI partitioning. THI partitioning is a measure of whether THI breaks down in the forward or reverse directions. The lack of effect from mutations

indicated that none of the residues catalyzes one step of the reaction, either addition or elimination, without affecting the other step (30). Other evidence includes: 1) These two residues are correctly situated for catalysis from the crystal structures; 2) THl partitioning is constant at higher pH, from pH 8 to 11.7, consistent with a single acid catalyst; 3) Glu341 is superposed with MurA\_Cys115, which is the proposed general acid/base catalyst for MurA reaction (30). This mechanism is consistent with the observed stereochemistry of *anti* addition and *syn* elimination.

Eschenburg et al. proposed a different set of catalytic residues based on the crystal structures, which gave rise to an opposite stereochemistry as *syn* elimination and *anti* addition as introduced above (25). They believed that Lys22 acted as both general acid and base in the addition step, transferring proton from 5-OH of S3P to C3 of PEP (25). In the elimination step, Asp313 was proposed to act as a general base, abstracting the proton from 4-OH which then deprotonate the C3' intramolecularly (25). No general acid for the elimination step was proposed.

Bartlett's group agreed with Mizyed that Glu341 acted as the proton donor for C3 in the addition step, however they believed that Asp313 was close enough to 5-OH of S3P to serve as the proton acceptor (24). Different from the above two groups, they proposed that during elimination step the phosphate itself acted as an intramolecular base, abstracting the proton from C3' to phosphate C-O bond (24). No enzymatic residues were directly involved. This mechanism also follows

the correct *anti* addition and *syn* elimination stereochemistry (24).

### Alternative reactions

The AroA reaction is fully reversible. In the reverse reaction, phosphate acts as the nucleophile to attack C2' of EPSP, yielding THI, which then breaks down to S3P and PEP (10). Our lab demonstrated that the reverse reaction proceeds through protonation at C3' and formation of a cationic intermediate (27). Since enzymes will employ the same TS structure for forward and reverse reactions, analyzing the reverse one could help to elucidate the intrinsic mechanism of AroA.

My project focuses on an alternative reverse reaction, AroA-catalyzed EPSP hydrolysis and its non-enzymatic counterpart, acid-catalyzed EPSP hydrolysis. Using H<sub>2</sub>O instead of Pi as the nucleophile makes the hydrolysis irreversible (Figure 6). It was determined that the first irreversible step in both reactions is C3' protonation, i.e. EPSP cation formation, since there was no <sup>1</sup>H exchange back into [3',3'-<sup>2</sup>H<sub>2</sub>]EPSP when it was hydrolyzed in regular water to 50% completion (31).

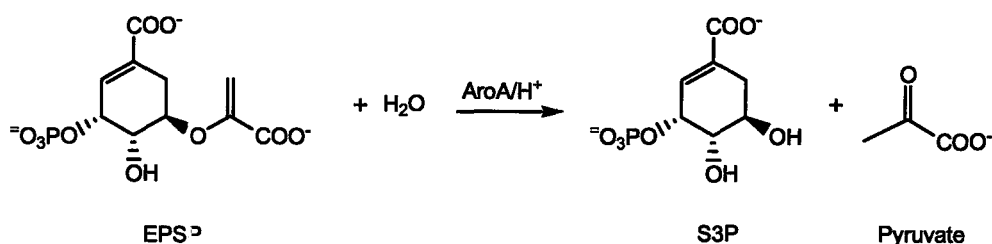


**Figure 6. AroA and acid catalyzed EPSP hydrolysis to S3P and pyruvate.**

The formation of EPSP ketal was observed in AroA's normal reverse

reaction and AroA-catalyzed EPSP hydrolysis, demonstrating the presence of EPSP cation in both reactions (27). EPSP ketal was not observed in acid-catalyzed hydrolysis, however it is possible that in solution the nucleophilic attack from H<sub>2</sub>O at C2' begins before C3' is fully protonated (27). EPSP ketal is highly unstable in solution as well. As a result, we believe that EPSP cation or a highly cationic TS is the common species among these reactions (Figure 7).

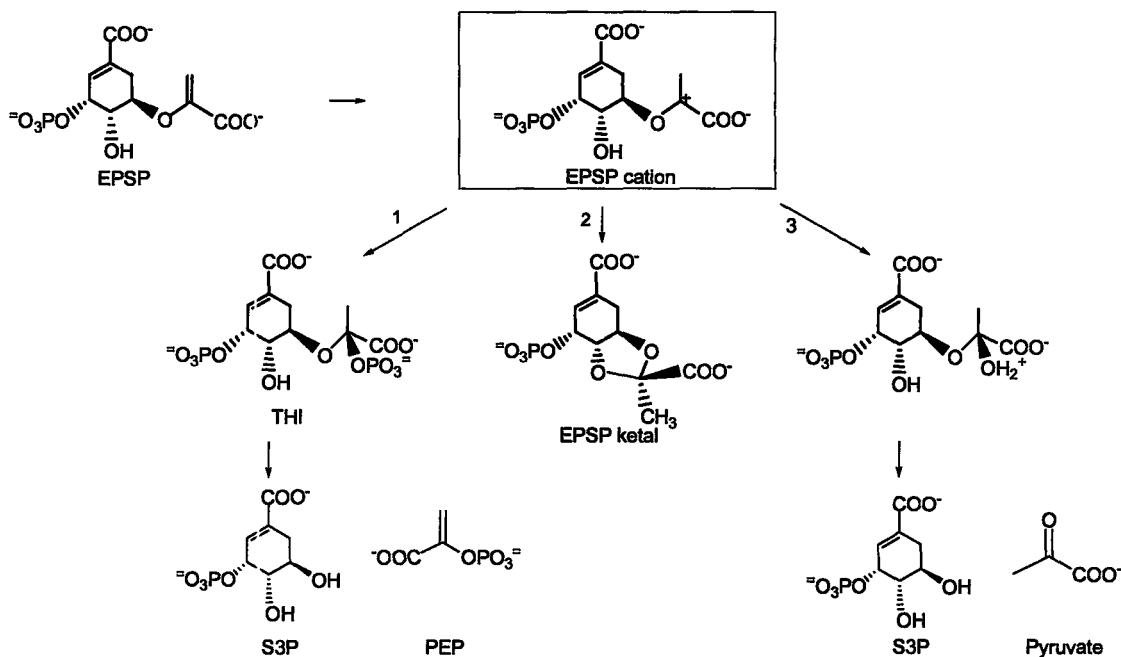


**Figure 7. EPSP cation as the common species for three pathways.** Pathway 1 is normal AroA reverse reaction from EPSP to S3P and PEP through THI; Pathway 2 yields a dead-end side product, EPSP ketal; Pathway 3 stands for AroA- or acid-catalyzed EPSP hydrolysis, producing S3P and pyruvate.

### Inhibitors of AroA reaction

The inhibition of AroA has been the subject of numerous studies, and many inhibitors have been reported in the literature, among which glyphosate is the best known one (6). Glyphosate is a competitive inhibitor with respect to PEP, and

uncompetitive with respect to S3P, possibly because it mimics the protonated form of PEP (Figure 8, 1, 2) (11).

Glyphosate's affinity for AroA was once thought to be due to it acting as a transition state analogue. However, this proposal was challenged by later experiments (7), including: 1) the hybrid of glyphosate and S3P, 4, is a modest inhibitor to AroA while the bisubstrate inhibitor containing S3P and a phosphonate analogue of PEP, 3, has a strong inhibitory impact (Figure 8, 3, 4); 2) glyphosate can still bind directly to the enzyme when the active site is occupied by EPSP; 3) there is no correlation between  $K_i$  and  $k_{cat}/K_m$  of a series of AroA mutants; while for a TS analogue inhibitor, any mutation that affects the catalytic efficiency ( $k_{cat}/K_m$ ) will interfere with its inhibitory potency ( $K_i$ ) (7). As a result it is a more prevailing opinion that glyphosate's inhibition is not directly related to any transition state structure.

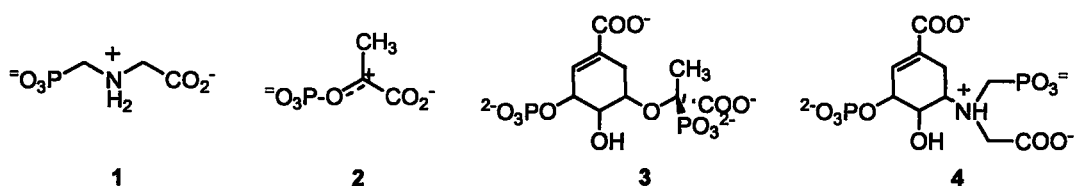
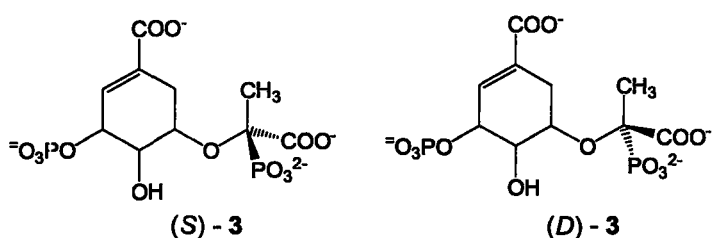


**Figure 8. Structures related to glyphosate.** 1. Structure of glyphosate; 2. Protonated PEP (*ref.* 11); 3. Bisubstrate inhibitor, a phosphonate THI analogue; 4. Hybrid of glyphosate and S3P (*ref.* 7).

Efforts are being made to find potent inhibitors that could act as antibiotics as well. A number of analogues of THI have been synthesized and screened, since AroA is expected to have a higher affinity for THI than substrates and

products (32). The *R*- and *S*-diastereomers of **3** were reported and evaluated as THI analogue inhibitors (33). They have  $K_{is}$  against EPSP of 15 nM and 1130 nM and  $K_{is}$  against Pi of 90 nM and 2100 nM, respectively (33). Surprisingly, the *R*-diastereomer is a better inhibitor even though the true THI has an *S* configuration (24).



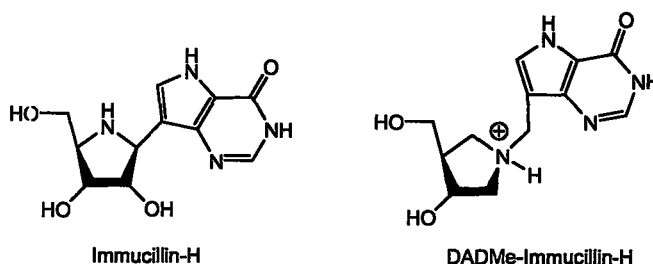
Glyphosate was introduced decades ago, yet all the efforts to develop analogues or molecular modification turned out to be unsuccessful. In contrast, resistance to penicillin was observed even before its clinical application, but  $\beta$ -lactams are still among the most commonly used antibiotics, because its mechanism is well understood. This phenomenon inspires scientists to explore more on the AroA mechanism.

### Transition state theory

A reaction coordinate diagram shows the energy changes along the reaction coordinate, in which the species corresponding to the highest energy point is defined as the transition state. According to the modern notion of enzyme catalysis, the TS, rather than reactants or products, has the optimal interaction with the enzyme (3). Enzymes promote reactions by lowering the activation energy through stabilizing the intrinsic TS structure or employing a different,

sometimes dramatically different, TS (3). As a result, a compound closely resembling the TS structure would have high affinity for the enzyme, making it a potent inhibitor.

Transition state studies can help to elucidate the intrinsic mechanism that enzymes employ to catalyze reactions. For example, Van Vleet discovered a carbanion transition state in the orotidine 5'-monophosphate decarboxylase reaction (34). He inferred that the enzyme promoted the reaction by destabilizing the ground-state by charge repulsion from Asp96, and stabilizing the TS with the positive charge of Lys93 (34). Moreover, enzyme inhibitors resembling TS structures have potential therapeutic application due to their extraordinary affinity with the enzyme (35). One case in point is the human purine nucleoside phosphorylase (36). Precise TS analysis made it possible to predict that DADMe-Immucillin-H would be a better inhibitor than the similar structure, Immucillin-H, since the TS employed a fully developed ribooxacarbenium ion and greater bond cleavage to the adenine group. DADMe-immucillin-H is now in phase 1b clinical trials for T-cell autoimmune disorders (35).



### Transition state and kinetic isotope effect (KIE)

Although the distinctive character of TS has caused tremendous interest,

its fleeting existence, about  $10^{-13}$  s, making conventional structure determination methods like crystallography or NMR no longer useful (3). One specific method for TS structure analysis is kinetic isotope effect (KIE) measurement. KIEs are defined as the ratio of rate constants for light and heavy isotopes:  $\text{KIE} = k_{\text{light}}/k_{\text{heavy}}$  (37). They measure the effect of isotopic substitution on the rate constants, reflecting the change in vibrational environment of labelled atoms between substrate and TS (37). If the labelled atom is involved in bond forming or breaking, such as C2' of EPSP, it is a primary KIE. If it is not directly involved in a chemical step, such as C1' of EPSP, this is a secondary KIE.

In a chemical reaction, if the vibrational environment becomes looser, such as when a bond is getting longer or broken, the lighter isotope will react faster, i.e.  $k_{\text{light}} > k_{\text{heavy}}$ , resulting in a normal KIE ( $\text{KIE} > 1.0$ ). Conversely, if the bond becomes shorter or stronger, leading to a tighter vibrational environment, the heavy isotope will react faster, i.e.  $k_{\text{light}} < k_{\text{heavy}}$ , and there will be an inverse KIE ( $\text{KIE} < 1.0$ ) (38). In this way, KIEs provide detailed information on single bond changes from substrate to TS.

Solvent deuterium KIEs (SDKIEs) are a special type of KIE. They are measured by running otherwise identical reactions in  $\text{H}_2\text{O}$  and  $\text{D}_2\text{O}$ . Their rate constants are compared to calculate SDKIE by equation 1.

$$\text{SDKIE} = k^{\text{H}}/k^{\text{D}} \quad (1)$$

SDKIE can tell us whether there is a solvent-based hydron<sup>1</sup> being transferred at the transition state. The SDKIE will be large if there is a proton “in flight” at the TS, making it a unique type of KIE.

### The sources of KIEs

KIEs arise from changes of vibrational frequency due to isotopic substitution. There are three factors that contribute to KIEs: changes in mass and moment of inertia (MMI), zero point energy (ZPE) and excited state energy (EXC) (37) (equation 2).

$$\text{KIE} = \text{MMI} * \text{ZPE} * \text{EXC} \quad (2)$$

The largest contribution to KIEs generally comes from ZPE. ZPE is the contribution from the change in vibrational energy at 0 K. At low temperatures, such as used here, bonds in the substrate remain in the lowest vibrational state, zero point energy accounts for most of their vibrational energy (38). At 0 K, zero point energy ( $E_0$ ) is defined by equation 3:

$$E_0 = \frac{h}{2} \sqrt{\frac{k}{\mu}} \quad (3),$$

where  $k$  is the force constant for stretching a bond, and  $\mu$  is the reduced mass,  $\mu = (m_1 * m_2) / (m_1 + m_2)$ , with  $m_1$  and  $m_2$  as the masses of the two atoms connected by the bond. Since  $E_0$  is inversely proportional to  $\mu$ , a lighter isotope will always have a larger  $E_0$  than a heavier one. For instance, the zero point energy of a C-H bond

---

<sup>1</sup> A hydron is an unspecified isotope of hydrogen (H, D or T). The elemental symbol for hydron is “L”.

is larger than the equivalent C-D bond in the labelled molecule.

Because  $E_0$  is also dependent on the strength of the bond, i.e. the force constant  $k$ , there will be an energy difference between the initial and final states,  $\Delta E_0$ . When these initial and final states are reactant and transition state of a reaction, the difference of  $\Delta E_0$  between light and heavy isotopes will affect their reaction rates, giving rise to a KIE (37). When a bond is getting weaker or broken, the force constant  $k$  decreases at TS. This will lead to a decrease in zero point energy at the TS, and the decrease is larger for the light isotope (Figure 9a). This results in a smaller activation energy barrier for the light isotope than the heavy one ( ${}^{\text{light}}\Delta E^\ddagger < {}^{\text{heavy}}\Delta E^\ddagger$ ), making the light isotope react faster. In this way zero point energy makes a normal contribution to the KIE. Conversely, when a bond is getting stronger or tighter at TS, zero point energy will increase more for the lighter isotope, resulting in slower reaction rate for the light isotope ( ${}^{\text{light}}\Delta E^\ddagger > {}^{\text{heavy}}\Delta E^\ddagger$ ), i.e. an inverse KIE (Figure 9b) (37).

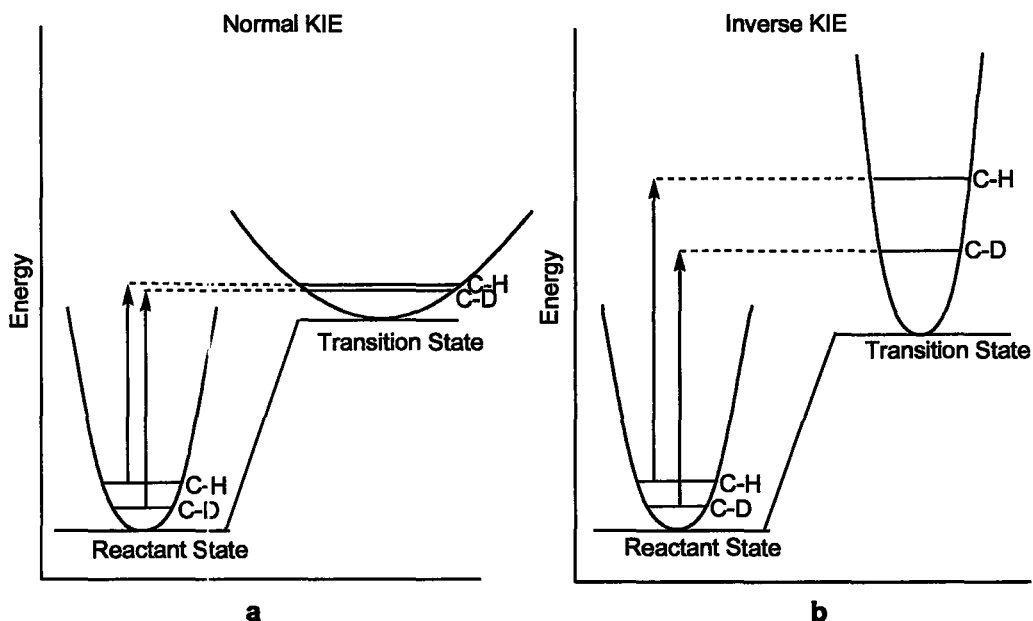


**Figure 9. Normal and inverse KIEs.** a). When there is a looser vibrational environment, force constant  $k$  decreases at TS, and there will be lower activation energy for the C-H bond, resulting in a normal KIE; b). Conversely, when there is a tighter vibrational environment, C-D bond has lower activation energy, leading to an inverse KIE. (ref. 37)

The contribution of MMI to KIE is from the change of mass and the moment of inertia in the labelled molecules. The EXC is from molecules that are vibrationally excited in the reactant. MMI and EXC are usually small compared with ZPE, though all of them are taken into account in computational KIEs (37).

Similar to KIEs, equilibrium isotope effects (EIEs) reflect the change in vibrational environment between reactants and products or intermediates. The difference lies in that a KIE includes the reaction coordinate motion at the TS. Since the structures of reactants and products can be determined by conventional methods, EIEs are easier to calculate computationally and can act as a reasonable estimate of some secondary KIEs which do not participate significantly

in the reaction coordinate motion (39).

### Methods to measure KIEs

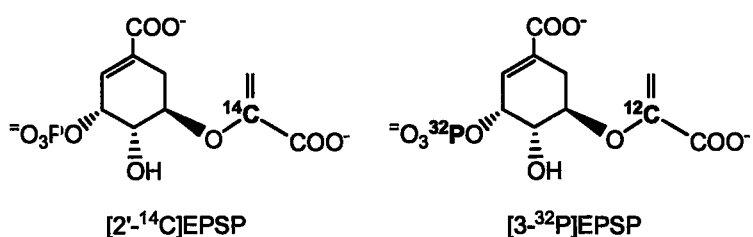
KIEs can be measured by either competitive or non-competitive methods. In a non-competitive measurement, the rate constants for the light and heavy isotopically labelled compounds are measured separately, and then their ratio is calculated. The advantage of non-competitive KIE measurement is that KIEs on any kinetic constant,  $k_{cat}$ ,  $k_{cat}/K_m$ , or  $K_m$  can be determined (40). However, the error from the constants measurement is generally too large for TS analysis. It is usually used for SDKIE measurement, which indicates whether or not there is proton transfer at the TS (40).

Competitive KIEs are measured by making a mixture of isotopically labelled substrates and reacting them competitively. If there is a KIE, the ratio of the isotopes will change during the course of the reaction. If the isotope ratio is being determined in the residual reactants, then it is measured at 0% reaction, which gives the initial isotope ratio, and at 50% reaction, when the ratio has changed. If the isotope ratio is being measured in the products, then it is measured at 100% reaction, which is equal to the initial isotope ratio, and at 50% reaction. The faster reacting isotope is enriched in the products while the slower one accumulates in the residual substrates (41). By avoiding direct measurement of rate constants, this competitive method is precise enough for TS analysis. It reports on the second-order rate constant of enzymatic reactions,  $k_{cat}/K_m$ , reflecting the first irreversible step (40). The most common technique for

competitive KIE measurement is using radioisotopes and liquid scintillation counting. The positions of interest are radiolabelled and the isotope ratios are determined. Another competitive way to measure KIEs is natural abundance NMR spectroscopy (39). Compared with the method of radioactivity, it removes the need for synthesizing radioactive compounds; however, it requires large amounts of material (39).

### Remote labels for KIE measurement by radioactivity

In a competitive KIE measurement, the sites of interest are labelled with two different isotopes and mixed together to measure the isotope ratio change. However, not all the isotopes, e.g.,  $^{12}\text{C}$ ,  $^{18}\text{O}$ ,  $^1\text{H}$  and  $^2\text{H}$ , are radioactive. Remote labels are therefore employed to report these stable isotopes so that the isotope ratio can be determined. For instance, in order to measure the  $[2'\text{-}^{14}\text{C}]$ EPSP KIE,  $[2'\text{-}^{14}\text{C}]$ - and  $[3\text{-}^{32}\text{P}]$ EPSP are synthesized, where  $[3\text{-}^{32}\text{P}]$  is a remote reporter for  $[2'\text{-}^{12}\text{C}]$ . As a result,  $^{12}\text{C}/^{14}\text{C}$  is represented by  $^{32}\text{P}/^{14}\text{C}$ , which can be determined by scintillation counting.



The criteria for remote label selection is that the  $E_{\text{max}}$  of the  $\beta$ -particles emitted from the two radionuclides are distinct, like  $^{32}\text{P}$  and  $^{14}\text{C}$  (Figure 10), so that it is possible to distinguish and quantify them in one solution by scintillation

counting.

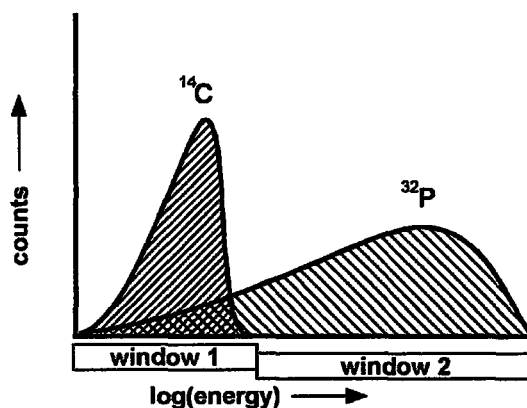


**Figure 10.**  $E_{\max}$  of the  $\beta$ -particle from  $^{14}\text{C}$  and  $^{32}\text{P}$ . Window 1 and 2 are set up following the  $E_{\max}$  of the  $\beta$ -particle of these two radionuclides. Window 1 contains all the counts from  $^{14}\text{C}$  as well as some from  $^{32}\text{P}$ . Window 2 contains counts from  $^{32}\text{P}$  only. Meanwhile, a standard sample containing  $^{32}\text{P}$  only is prepared in the same buffer to calculate the proportion of  $^{32}\text{P}$  counts in window 1. In this way,  $^{14}\text{C}$  and  $^{32}\text{P}$  are well separated and quantified.

### Computational EIEs/KIEs

Experimental KIEs reflect the change in vibrational environment between reactants and TS; however, they cannot predict the TS structures directly. Instead, putative TS candidates are proposed computationally and their KIEs are calculated to compare with the experimental values. The best match between these two values gives the correct experimental TS structure.

EIEs can be described in equation 4 (41).

$$\text{EIE} = \text{MMI} * \text{ZPE} * \text{EXC} \quad (4)$$

When EIEs are calculated computationally, the contribution from EXC, ZPE and MMI can be described by equation 5 to 7 (41),

$$\text{EXC} = \frac{\left[ \prod_i^{3N-6} \frac{1 - e^{(-heavy u_i)}}{1 - e^{(-light u_i)}} \right]_{final}}{\left[ \prod_i^{3N-6} \frac{1 - e^{(-heavy u_i)}}{1 - e^{(-light u_i)}} \right]_{initial}} \quad (5),$$

$$\text{ZPE} = \frac{\left[ \prod_i^{3N-6} e^{-(light u_i - heavy u_i)/2} \right]_{final}}{\left[ \prod_i^{3N-6} e^{-(light u_i - heavy u_i)/2} \right]_{initial}} \quad (6),$$

$$\text{MMI} = \frac{\left( \prod_i^{3N-6} \frac{light u_i}{heavy u_i} \right)_{final}}{\left( \prod_i^{3N-6} \frac{light u_i}{heavy u_i} \right)_{initial}} \quad (7),$$

where  $u_i = hv_i/k_B T$ ,  $h$  is Planck's constant,  $v_i$  is the vibrational frequency which can be calculated from each molecular structure,  $k_B$  is Boltzmann's constant,  $T$  is temperature, and  $3N-6$  is the number of vibrational frequencies for each molecule. Final and initial states here refer to intermediates and reactants respectively.

KIEs can be calculated mathematically in a similar way using a computationally optimized TS structure. Equations 5 to 7 have to be modified to apply to KIEs since the TS has  $3N-7$  vibrational frequencies rather than  $3N-6$ . The remaining vibrational mode in the TS is the reaction coordinate, which has an imaginary frequency. The reaction coordinate motion always makes a normal contribution to the MMI (equation 8) (41).

$$\text{MMI} = \frac{\text{light } \nu^*}{\text{heavy } \nu^*} \times \frac{\left( \prod_i^{3N-7} \frac{\text{light } \omega_i}{\text{heavy } \omega_i} \right)_{\text{TS}(\text{final})}}{\left( \prod_i^{3N-6} \frac{\text{light } \omega_i}{\text{heavy } \omega_i} \right)_{\text{initial}}} \quad (8),$$

where  $\text{light } \nu^*/\text{heavy } \nu^*$  is the reaction coordinate motion.

Computational KIEs are obtained by first computationally optimizing the structures of the reactant and transition state. Vibrational frequencies are then calculated from the optimized structures. KIEs are calculated using the program *QUIVER*, which re-calculates vibrational frequencies of isotopically labelled compounds from the optimized structures, and from there, KIEs. Computational EIEs are calculated in the same way, except that the relevant species are the reactant and product.

### Objective of this project

The goal of this project was to determine the KIEs of AroA- and acid-catalyzed EPSP hydrolysis, and analyze their transition state structures. A series of radiolabelled EPSPs would be synthesized and the conditions for KIE measurement would be developed. KIEs for AroA- and acid-catalyzed EPSP hydrolysis would then be determined competitively. Computational TS structures would be set up and their theoretical KIEs calculated to compare with the experimental data. KIEs can provide a better picture of AroA's catalytic mechanism, such as whether it employs a concerted or stepwise addition. The accurate prediction of TS structures from TS analysis will shed light on the design

of TS-like AroA inhibitors, thus promoting the development of novel antimicrobial drugs, and herbicides.

## **Methods**

### **General**

All reagents were purchased from Sigma-Aldrich or Bioshop Canada unless otherwise noted. [1-<sup>14</sup>C]pyruvate was from GE Healthcare, while [2-<sup>14</sup>C]pyruvate and [3-<sup>14</sup>C]pyruvate were from American Radiolabelled Chemicals Incorporation. [ $\gamma$ -<sup>33</sup>P]ATP and [ $\gamma$ -<sup>32</sup>P]ATP were purchased from Perkin Elmer. <sup>2</sup>H<sub>2</sub>O was from Cambridge Isotope Labs. Mono Q™ 5/50 GL and chelating Sepharose columns were from GE Healthcare and the C-18 reverse phase column was from Waters Ltd.. HPLC chromatography was performed on a Waters system equipped with a dual UV wavelength detector. Radioactivity was quantified with a Beckman LS 6500 liquid scintillation counter.

### **Protein purification**

*E. coli* AroA bearing a C-terminal His-tag was expressed and purified as described previously (30). A pET24d vector containing AroA fragment was transformed into BL21\*(DE3) by electroporation. A single colony was selected and cultivated overnight at 37 °C in 25 mL LB media with 50 µg/mL kanamycin. The overnight culture was inoculated into 1L fresh LB media with 50 µg/mL kanamycin and grown for another 4 hours until OD<sub>600</sub> reached 0.6. AroA expression was induced with 1 mM isopropyl-β-d-thiogalactopyranoside (IPTG) for 4 hours at 37 °C. The cells were then harvested by centrifuging at 10,000 x g for 10 min, and the pellet was re-suspended in 20-30 mL lysis buffer containing 50 mM Tris-HCl,

pH 7.5, 300 mM NaCl and 20 mM imidazole. Cells were lysed in a French Press after addition of 100 µg/mL DNAase and RNAase and 1 mM phenylmethylsulfonyl fluoride (PMSF). Cell debris was removed by centrifuging at 20,000 x g for 20 min. The supernatant was applied to chelating-Sepharose column charged with NiSO<sub>4</sub>. Non-specifically bound proteins were eluted with lysis buffer, and then AroA was eluted with elution buffer (lysis buffer but with 500 mM imidazole). After purification AroA was concentrated and exchanged into storage buffer (50 mM HEPES, pH 7.5, 50 mM KCl) by ultrafiltration with a YM10 membrane (Millipore Corp.).

A plasmid containing the phosphoenolpyruvate synthetase (ppsA) gene was a generous gift from Dr. David Jakeman (Dalhousie University). ppsA was overexpressed and purified as described previously (42). After French Press lysis, the protein was precipitated with ammonium sulfate at 40% saturation. The pellet was removed by centrifugation, at 11,000 x g for 15 min. More ammonium sulfate was added to 50% saturation and the precipitate was collected by centrifugation. The protein was re-dissolved in buffer (50 mM Tris-HCl, pH 6.8, 1 mM DTT, 1.5 mM NaN<sub>3</sub>), and the ppsA concentration was determined using Bio-rad assay with bovine serum albumin (BSA) as standard (42).

### **Characterization of purified AroA**

The protein concentration of AroA was determined by UV absorbance at 280 nm using  $\epsilon_{280} = 3.55 \times 10^4 \text{ M}^{-1} \text{ cm}^{-1}$  (30,43).

The concentration of active AroA was measured by fluorescence titration

with S3P (30,44). The assay is based on the fact that S3P, in the presence of glyphosate, has a high affinity with AroA and its binding causes a decrease in intrinsic Trp fluorescence. A 2 mL solution of 50 mM HEPES, pH 7.0, 50 mM KCl, 500  $\mu$ M glyphosate and 1  $\mu$ M AroA was prepared and 30  $\mu$ M S3P was used to titrate it. The excitation wavelength was 280 nm while the emission was 360 nm. Aliquots (10  $\mu$ L) of S3P were added and the fluorescence reading recorded once it was constant. The dilution effect was corrected and the active concentration of AroA can be calculated since the binding ratio of S3P and AroA is 1.

AroA's catalytic activity was followed by the rate of Pi formation in the forward reaction using the Malachite Green / ammonium molybdate (MG/AM) assay for Pi (45). Aliquots of reaction mixture (10  $\mu$ L) were added to 50  $\mu$ L MG/AM (0.063% Malachite Green, 2.1% ammonium molybdate, 2 M HCl), followed 90 s later by 10  $\mu$ L 34% sodium citrate. The absorbance at 660 nm was read within 30 min to find the Pi concentration. AroA's reaction contained 50 mM K-HEPES, pH 7.0, 1 mM S3P, 5 mM PEP and 10 nM AroA.

### **EPSP synthesis and hydrolysis**

EPSP was synthesized using 1  $\mu$ M AroA, 1 mM S3P and 2 mM PEP. The reaction was >90% completion after overnight incubation at 37 °C. EPSP was purified by anion exchange chromatography on a Mono Q column with a gradient of 100 mM to 700 mM ammonium bicarbonate, pH 10.0, over 50 min at a flow rate of 0.5 mL/min and  $A_{240}/A_{280}$  detection. EPSP eluted at 35 min. EPSP was then lyophilized to remove the volatile salts and re-dissolved in H<sub>2</sub>O.

Low concentrations of Pi are ubiquitous in solution. In order to ensure that the normal AroA reverse reaction did not compete with EPSP hydrolysis, a Pi scavenging system developed by Meghann Clark was used on reaction solutions (31). The Pi scavenging system consisted of 50 mM Tris-HCl, pH 7.5, 50  $\mu$ M KCl, 50  $\mu$ M MgCl<sub>2</sub>, 10 U/mL sucrose phosphorylase (SP), 1 mM sucrose, 0.2 mM NADP, 10 U/mL phosphoglucomutase (PGM) and 10 U/mL glucose 6-phosphate dehydrogenase (G6PDH), which could remove almost all the Pi in solution by turning Pi and sucrose into 6-phosphogluconate irreversibly (31).

AroA-catalyzed EPSP hydrolysis reactions contained 50  $\mu$ M AroA, 500  $\mu$ M EPSP and 50 mM Tris-HCl, pH 7.5. Acid-catalyzed EPSP hydrolysis was performed with 500  $\mu$ M EPSP in 50 mM ammonium acetate, pH 5.4, at 90 °C.

### **SDKIE of AroA-catalyzed EPSP hydrolysis**

The SDKIE of AroA-catalyzed EPSP hydrolysis was measured from the rates of EPSP hydrolysis in H<sub>2</sub>O and D<sub>2</sub>O. The reaction mixture contained 50  $\mu$ M AroA, 500  $\mu$ M EPSP, 50 mM Tris-HCl, pH 7.5, and the Pi scavenging system. For the D<sub>2</sub>O reaction, Tris solid and Pi scavenging mixture were dissolved directly in D<sub>2</sub>O and pH was adjusted with DCl or NaOD. EPSP was exchanged into D<sub>2</sub>O by lyophilization while AroA in D<sub>2</sub>O was obtained via G25 spin column (GE Healthcare) to maintain its activity. The spin column was pre-equilibrated by either Tris-H<sub>2</sub>O or Tris-D<sub>2</sub>O, and then 50  $\mu$ L aliquots of AroA were applied. The columns were centrifuged at 735 x g for 2 min. Eluted AroA was quantified by A<sub>280</sub>. <sup>1</sup>H-NMR was employed to monitor the amount of residual <sup>1</sup>H in the D<sub>2</sub>O solution.

EPSP and AroA were incubated with the Pi scavenging system separately at 37 °C for 45 min before being mixed together to start EPSP hydrolysis. At each time point, 50  $\mu$ L aliquots of reaction mixture were taken and diluted to 100  $\mu$ L with H<sub>2</sub>O, and 100  $\mu$ L of 0.4 N KOH was added to quench the reaction. The denatured protein was removed by centrifugal ultrafiltration over Microcon YM 10 membranes (Millipore Corp.) at 14,000 x g for 1 h. A 150  $\mu$ L aliquot of the filtrate was recovered and the extent of reaction quantified by anion exchange HPLC under the same conditions as EPSP purification. Time points up to 6 h were collected. The ratios of  $\epsilon_{240}$  for S3P:PEP:EPSP was 0.59:1:2.1 (10). The observed rate was assumed to be the initial rate because [EPSP]  $\gg$   $K_m$  and  $k_{cat}$  can be calculated from equation 9:

$$V = k_{cat} * [E] \quad (9).$$

The SDKIEs were calculated from the rate constants for the H<sub>2</sub>O and D<sub>2</sub>O reactions, using equation 10:

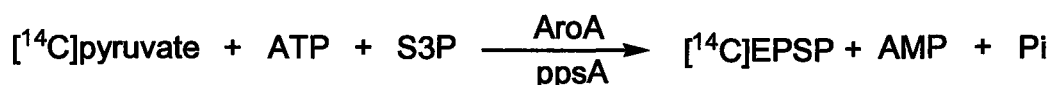
$$\text{SDKIE} = {}^H k_{cat} / {}^D k_{cat} \quad (10).$$

### Synthesis of radiolabelled EPSPs

[1'-<sup>14</sup>C]-, [2'-<sup>14</sup>C]- and [3'-<sup>14</sup>C]EPSP were synthesized by coupled reactions of ppsA and AroA from S3P and [1-<sup>14</sup>C]-, [2-<sup>14</sup>C]- or [3-<sup>14</sup>C]pyruvate (Scheme 1). The reaction mixture contained 50 mM Tris-HCl, pH 7.5, 5 mM KCl, 10 mM MgCl<sub>2</sub>, 10 mM pyruvate (10  $\mu$ Ci), 15 mM ATP, 12 mM S3P, 15 mg/mL ppsA and 1  $\mu$ M AroA. 1 M KOH was used to adjust pH to above 7.5. The reaction was incubated

at 37 °C overnight and typically reached around 80% completion. Labelled EPSPs were then purified by HPLC in the same manner as above. Their concentration and specific activity were determined by analytical HPLC and liquid scintillation counting respectively. The reaction was shown as below:

### Scheme 1.



$[^{32}\text{P}]$ - and  $[^{33}\text{P}]\text{EPSP}$  were synthesized from shikimic acid and labelled ATP with a combination of AroK (shikimate kinase) and AroA (Scheme 2). The reaction contained 50 mM Tris-HCl, pH 7.5, 50 mM KCl, 10 mM MgCl<sub>2</sub>, 25 mM sodium tungstate, 10 mM shikimic acid, 10 mM PEP, 2 mM  $[\gamma\text{-}^{32}\text{P}]$  or  $[\gamma\text{-}^{33}\text{P}]\text{ATP}$  (25  $\mu\text{Ci}$ ), 1  $\mu\text{M}$  AroA, and 100  $\mu\text{L/mL}$  AroK. The pH was adjusted to above 7.5 by KOH and the reaction was diluted by 10-fold with H<sub>2</sub>O to eliminate the product inhibition from ADP. After overnight incubation at 37 °C, the reaction typically reached around 70% completion.  $[^{32}\text{P}]$ - and  $[^{33}\text{P}]\text{EPSP}$  were purified and quantified in the same way as the  $[^{14}\text{C}]\text{EPSPs}$ .

### Scheme 2.

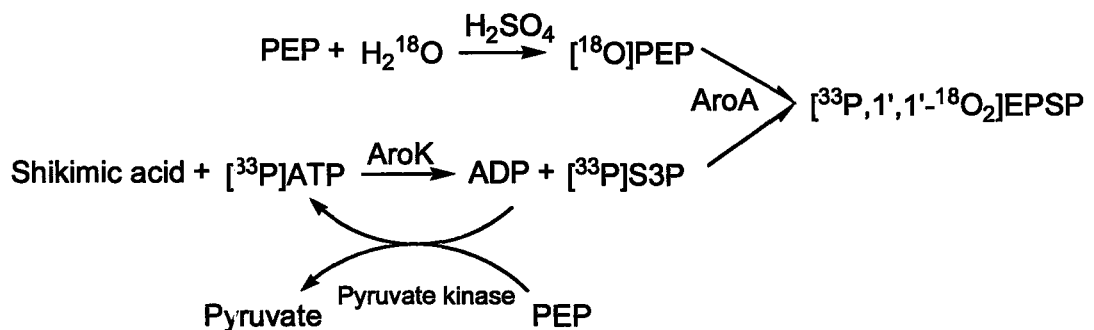


$[^{33}\text{P}, 5\text{-}^{18}\text{O}]\text{EPSP}$  synthesis employed the same AroK and AroA reactions as  $[^{33}\text{P}]\text{EPSP}$ , except using  $[5\text{-}^{18}\text{O}]\text{shikimic acid}$ .  $[5\text{-}^{18}\text{O}]\text{shikimic acid}$  was synthesized by Vivian Gawuga in our lab by conventional organic synthesis. A parallel reaction with  $[5\text{-}^{18}\text{O}]\text{shikimic acid}$  but non-radioactive ATP was run under

the same conditions to monitor the extent of  $^{18}\text{O}$  enrichment by mass spectrometry without having to introduce  $^{33}\text{P}$  contamination into the mass spectrometer.

$[^{33}\text{P},3',3'\text{-}^2\text{H}_2]\text{EPSP}$  was synthesized by making  $[^{33}\text{P}]\text{EPSP}$  as described above, then incubating with  $1\ \mu\text{M}$  AroA and  $5\ \text{mM}$  Pi overnight in  $\text{D}_2\text{O}$ . The AroA reaction is freely reversible and equilibrium favours the forward direction by a factor of 15.  $[^{33}\text{P},3',3'\text{-}^2\text{H}_2]\text{EPSP}$  was quantified by liquid scintillation counting and the extent of  $^2\text{H}$  incorporation was determined by mass spectrometry of a parallel reaction run under identical conditions using unlabelled EPSP.

$[^{33}\text{P},1',1'\text{-}^{18}\text{O}_2]\text{EPSP}$  was synthesized from  $[^{33}\text{P}]\text{S3P}$  and  $[^{18}\text{O}]\text{PEP}$  (Scheme 3).  $[^{33}\text{P}]\text{S3P}$  was produced by AroK reaction using  $50\ \text{mM}$  Tris-HCl, pH 7.5,  $50\ \text{mM}$  KCl,  $10\ \text{mM}$   $\text{MgCl}_2$ ,  $25\ \text{mM}$  sodium tungstate,  $20\ \text{mM}$  shikimic acid,  $10\ \text{mM}$  PEP,  $60\ \text{U/mL}$  pyruvate kinase,  $2\ \text{mM}$   $[\gamma\text{-}^{33}\text{P}]\text{ATP}$  ( $25\ \mu\text{Ci}$ ), and  $100\ \mu\text{L/mL}$  AroK. PEP and pyruvate kinase were used to recycle ADP to ATP.  $[^{33}\text{P}]\text{S3P}$  was purified by HPLC and the solvent removed by lyophilization. Meanwhile, the carboxylate oxygens in  $90\ \text{mM}$  PEP was exchanged with  $\text{H}_2^{18}\text{O}$ , catalyzed by  $1.5\ \text{M}$   $\text{H}_2\text{SO}_4$  at  $95\ ^\circ\text{C}$  for  $30\ \text{min}$ . The neutralized PEP product was divided equally into two portions, of which one reacted with  $[^{33}\text{P}]\text{S3P}$  to produce  $[^{33}\text{P},1',1'\text{-}^{18}\text{O}_2]\text{EPSP}$  while the other one was used in a parallel reaction to form  $[1',1'\text{-}^{18}\text{O}_2]\text{EPSP}$ . Mass spectrometry of  $[1',1'\text{-}^{18}\text{O}_2]\text{EPSP}$  gave the extent of  $^{18}\text{O}$  enrichment, while liquid scintillation counting was used to quantify  $[^{33}\text{P},1',1'\text{-}^{18}\text{O}_2]\text{EPSP}$ .

**Scheme 3.****KIE measurement for AroA-catalyzed EPSP hydrolysis**

KIEs were measured using the competitive method. EPSP (0.25  $\mu\text{Ci}$  each of two different radiolabels) was re-purified by C-18 reverse phase HPLC using isocratic elution in 50 mM ammonium acetate, pH 6, 44 mM KCl and 2.5 mM tetrabutylammonium sulfate (TBAS). Re-purified EPSP was lyophilized and re-dissolved in  $\text{H}_2\text{O}$ . Each reaction contained 50 mM Tris-HCl, pH 7.5, 500  $\mu\text{M}$  EPSP, 50  $\mu\text{M}$  AroA and the Pi scavenging mixture in a 300  $\mu\text{L}$  solution. EPSP and AroA were incubated with Pi scavenging system separately at 37  $^\circ\text{C}$  for 30 min before being mixed together. A 100  $\mu\text{L}$  aliquot of the reaction was quenched immediately by heating at 95  $^\circ\text{C}$  and used as 0% extent; while the rest was incubated at 37  $^\circ\text{C}$  until it reached around 50% completion. Both 0% and 50% reactions were injected separately on a Mono Q column with a gradient of 100 mM to 500 mM KCl in 10 mM  $\text{NH}_4\text{Cl}$ , pH 10.0 at 0.5 mL/min over 26 min. The entire peaks of S3P, pyruvate and remaining EPSP were collected. The liquid weight of each peak was adjusted to be equal to that of EPSP using 298 mM KCl and 10 mM  $\text{NH}_4\text{Cl}$ , the buffer concentration at which EPSP eluted. Each peak was split

equally into two scintillation vials, and neutralized with 100  $\mu\text{L}$  of potassium phosphate, pH 6.0 before 20 mL Liquiscint was added. A blank sample and a  $^{32}\text{P}$  standard were prepared with an appropriate volume of 298 mM KCl and 10 mM  $\text{NH}_4\text{Cl}$ . Each vial was counted for 10 min repeatedly until the 95% confidence interval of the KIE was  $< 0.005$ .

The extent of the reaction was calculated by comparing the radioactivity in S3P and pyruvate with the remaining EPSP. The isotope ratios in the residual EPSP at 0% and 50% were also determined to calculate KIEs by equation 11:

$$KIE = \frac{\ln \left[ \frac{(1-f)(1 + \frac{\text{heavy } S_0}{\text{light } S_0})}{1 + \frac{\text{heavy } S_i}{\text{light } S_i}} \right]}{\ln \left[ \frac{(1-f)(1 + \frac{\text{light } S_0}{\text{heavy } S_0})}{(1 + \frac{\text{light } S_i}{\text{heavy } S_i})} \right]} \quad (11),$$

where  $f$  is the extent of reaction,  $S_0$  is the light or heavy isotope at the beginning of the reaction, and  $S_i$  is the light or heavy isotope at  $f$  extent of the reaction (39).

### **KIE measurement for acid-catalyzed EPSP hydrolysis**

The protocol for measuring KIEs of acid-catalyzed reaction was developed by Ayesha Malik from our lab, based on my method for the AroA-catalyzed reaction. Labelled EPSP was re-purified by reverse phase HPLC. The collected peak, around 2 mL., was adjusted to pH  $5.40 \pm 0.03$  with HCl and divided into two portions. One third was injected directly to Mono Q column as 0% extent, while the rest was incubated at  $90^\circ\text{C}$  for 50 min to reach around 50% extent of reaction. No

Pi scavenging system was required. The rest of the procedure was the same

### **Testing KIE measurement method**

Radioisotopes are distinguished in scintillation counting by the differences in the energy of their  $\beta$ -particles. Samples of 0.05  $\mu$ Ci of  $^{14}\text{C}$ ,  $^{32}\text{P}$ , or  $^{33}\text{P}$  were diluted in 20 mL Liquiscint fluid (National Diagnostic) and  $\beta$ -particle energy spectra were determined. Spectral windows were selected so that all of the radioactive decay events of the lower energy radionuclide ( $^{14}\text{C}$  or  $^{33}\text{P}$ ) were detected in window 1, along with some counts from the higher energy radionuclide ( $^{32}\text{P}$ ). Window 2 contained counts only from  $^{32}\text{P}$ .

The efficiency of Pi scavenging was tested by incubating EPSP or AroA with the Pi scavenging mixture at 37 °C for 30 min, then determining the residual Pi in solution by the MG/AM assay.

Complete radioisotope chromatograms were collected to ensure that the expected products were found, and there were no unanticipated radioactive products or side products. A mixture of [ $^{14}\text{C}$ ]- and [ $^{32}\text{P}$ ]EPSP was reacted and purified as for a KIE measurement. Both 0% and 50% reactions were applied to a Mono Q column and 0.25 mL fractions were collected and counted after dilution with 10 mL of Liquiscint.

The effect of chromatography on the isotope ratio was checked. A sample containing [ $^{14}\text{C}$ ]- and [ $^{32}\text{P}$ ]EPSP was injected onto HPLC. The entire EPSP peak was collected and divided into two parts. One was diluted in 20 mL Liquiscint and

counted directly, while the other portion was injected back onto the HPLC and the EPSP peak was collected and counted as for the first run. The  $^{14}\text{C}/^{32}\text{P}$  ratios from these two peaks were compared to detect any isotope fractionation upon chromatography.

### Computational EIE/KIE calculation

Computational EIEs and KIEs are calculated based on the structures and vibrational frequency of EPSP, EPSP cation and the candidate TS. To simplify the models for EPSP and oxacarbenium ion, we replaced shikimate with a methyl group because KIEs are not affected by distant atoms (Figure 11). The *enol*/pyruvyl methane structure is stable; while for the cationic structure, the negatively charged carboxylate group tends to attack C2', forming an  $\alpha$ -lactone. Thus, other molecules, such as  $\text{H}_2\text{O}$ , lithium or guanidinium ion, were added to stabilize the oxacarbenium ion.

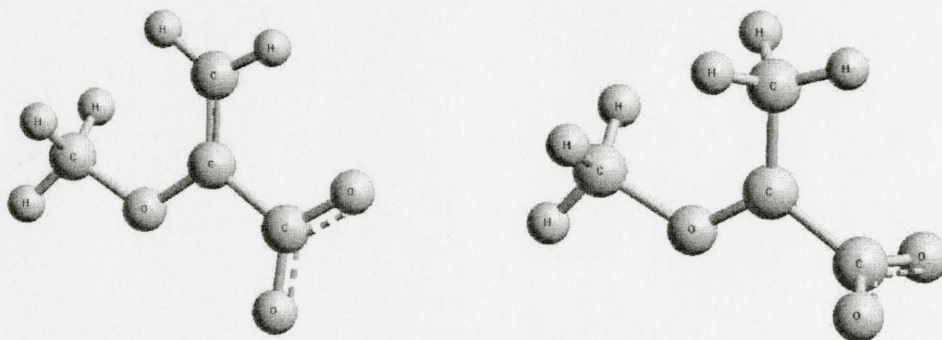


**Figure 11. Computational structures for KIE/EIE calculation.** *Enol*/pyruvyl methane and its protonated form stand for the structures of EPSP and oxacarbenium ion.

Computational transition states were found for proton transfer at C3', by my supervisor, Dr. Paul Berti.

Optimization and frequency calculation were performed with Gaussian 03 using hybrid density functional theory and a 6-31+G\*\* basis set (RB3PW91/6-31+G\*\*), and were used to calculate EIEs/KIEs by *QUIVER* (46). As for EIE calculation, the fractionation factors ( $Q$ ) were determined at 310 K for AroA-catalyzed hydrolysis and 363 K for acid-catalyzed reaction. EIEs at each labelled position were obtained by dividing  $Q$  of the reactant by  $Q$  of the intermediate, that is,  $EIE = Q_{\text{reactant}}/Q_{\text{intermediate}}$ . Similarly, KIEs were calculated by determining the  $Q$  from the reactant and TS. However, due to the contribution of reaction coordinate motion to KIEs, another factor of  $\frac{\nu_{\text{light}}^*}{\nu_{\text{heavy}}^*}$  need to be taken into consideration, i.e.  $KIE = Q_{\text{reactant}}/Q_{\text{TS}} * \frac{\nu_{\text{light}}^*}{\nu_{\text{heavy}}^*}$ .

## Results

### **AroA purification**

AroA<sub>H6</sub> was expressed and purified from *E. coli*. Its purity, as determined by SDS/PAGE, was routinely >98%. The protein concentration was determined from A<sub>280</sub>. The concentration of active AroA was measured by fluorescence titration. In the presence of excess glyphosate, S3P binds tightly with AroA in a 1:1 ratio, causing the closure of AroA's active site and a decrease in Trp fluorescence. The point at which fluorescence stops decreasing is where S3P's concentration equals to AroA's concentration. The intersection of the two lines was the active concentration of AroA. Active AroA was around 70% of the total protein (Figure 12).

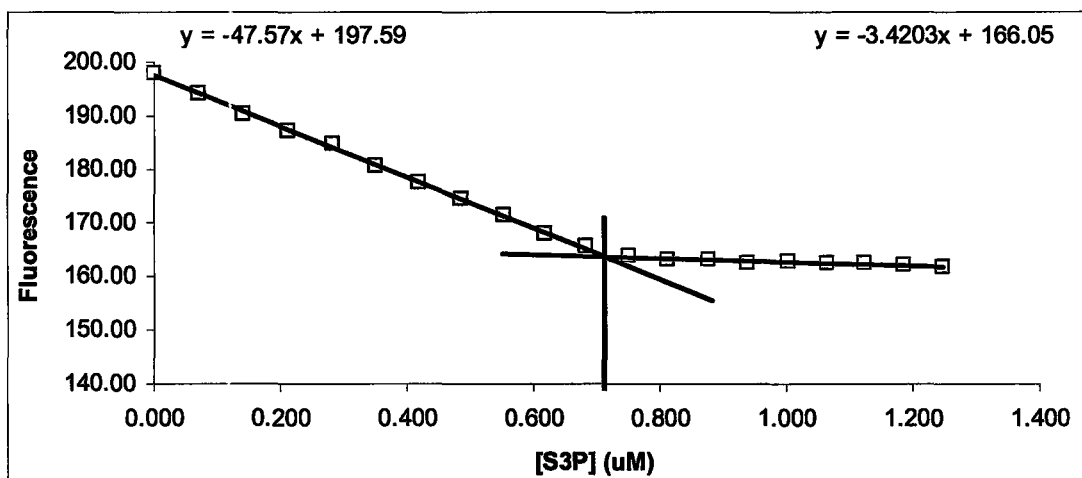


**Figure 12. Fluorescence titration for AroA active concentration.** AroA (1 µM protein concentration) was titrated with 30 µM S3P until it was saturated. The active AroA concentration in this sample was 0.71 µM.

Reaction rates were measured by colorimetric detection of Pi formation

with the MG/AM assay. With saturating substrate concentrations, the initial velocity with 10 nM AroA was  $300 \text{ nM} \cdot \text{s}^{-1}$  (Figure 13), or  $v_0/[E_0] = 30 \text{ s}^{-1}$ . This was consistent with the literature  $k_{\text{cat}}$  value of  $30 \text{ s}^{-1}$ , indicating the enzyme was fully functional (6).

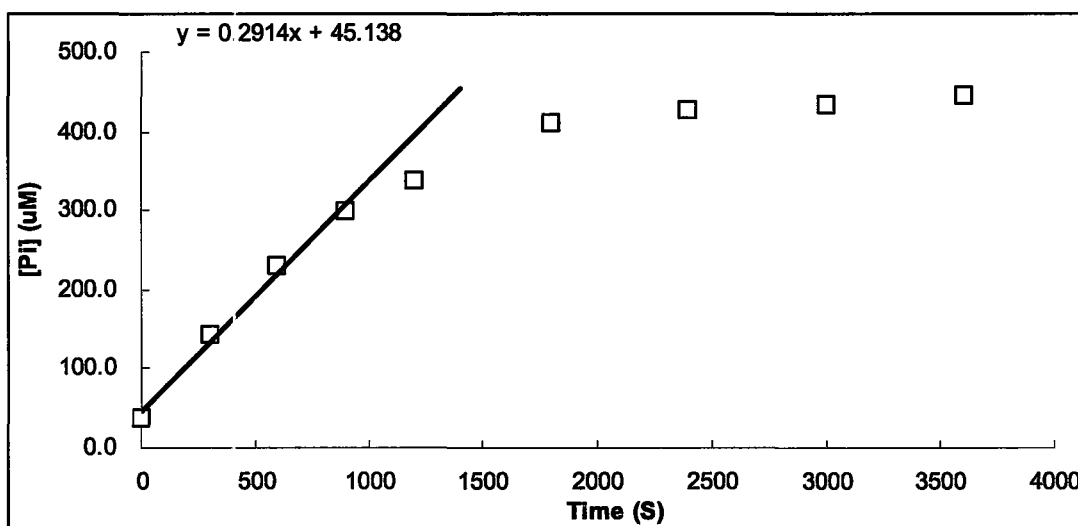


**Figure 13. MG/AM assay for AroA activity.** The initial velocity with 10 nM AroA was  $300 \text{ nM} \cdot \text{s}^{-1}$ .

### **SDKIE of AroA-catalyzed EPSP hydrolysis**

The SDKIE of AroA-catalyzed EPSP hydrolysis was measured by the non-competitive method, in which the rates of EPSP hydrolysis in  $\text{H}_2\text{O}$  and  $\text{D}_2\text{O}$  were measured separately and compared. AroA was exchanged into  $\text{D}_2\text{O}$  by gel filtration in a G25 spin column, and  $^1\text{H-NMR}$  was used to monitor the residual H. After exchange, the solvent had 1.6% H, a negligible amount (data not shown). Reaction rates in  $\text{H}_2\text{O}$  and  $\text{D}_2\text{O}$  were determined by following either EPSP disappearance or S3P production by HPLC in the first 6 hours of the reaction (Figure 14).

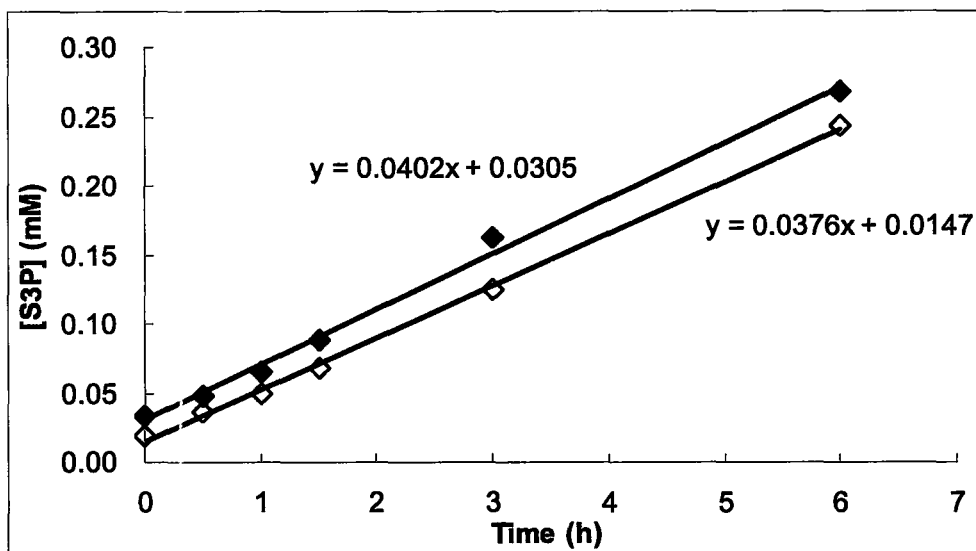


**Figure 14. Rates of S3P production in one individual trial.** The reactions were run in either H<sub>2</sub>O (open diamonds) or D<sub>2</sub>O (filled diamonds) at 37 °C for 6 h and the rates were fitted into a linear curve.

As  $K_d_{\text{EPSP}} \approx 1 \mu\text{M}$  (6) and  $[\text{EPSP}] = 500 \mu\text{M}$  in the SDKIE measurements, the rate reflected  $k_{\text{cat}}$  of EPSP hydrolysis (Table 1).

**Table 1. SDKIE for AroA-catalyzed EPSP hydrolysis**

Trials	Trial 1		Trial 2	
	H <sub>2</sub> O	D <sub>2</sub> O	H <sub>2</sub> O	D <sub>2</sub> O
Slope	18.89 nM·s <sup>-1</sup>	18.83 nM·s <sup>-1</sup>	10.44 nM·s <sup>-1</sup>	11.17 nM·s <sup>-1</sup>
$k_{\text{cat}}^a$	3.78*10 <sup>-4</sup> s <sup>-1</sup>	3.77*10 <sup>-4</sup> s <sup>-1</sup>	2.09*10 <sup>-4</sup> s <sup>-1</sup>	2.23*10 <sup>-4</sup> s <sup>-1</sup>
SDKIE	0.99		0.94	
Mean <sup>b</sup>	0.97 ± 0.04			

<sup>a</sup>  $[\text{AroA}] = 50 \mu\text{M}$ ,  $k_{\text{cat}} = v_0/[\text{AroA}]$

<sup>b</sup> Mean of two individual trials ± standard deviation.

### Synthesis of radiolabelled EPSPs

A series of radiolabelled EPSPs were synthesized (Figure 15, Table 2).

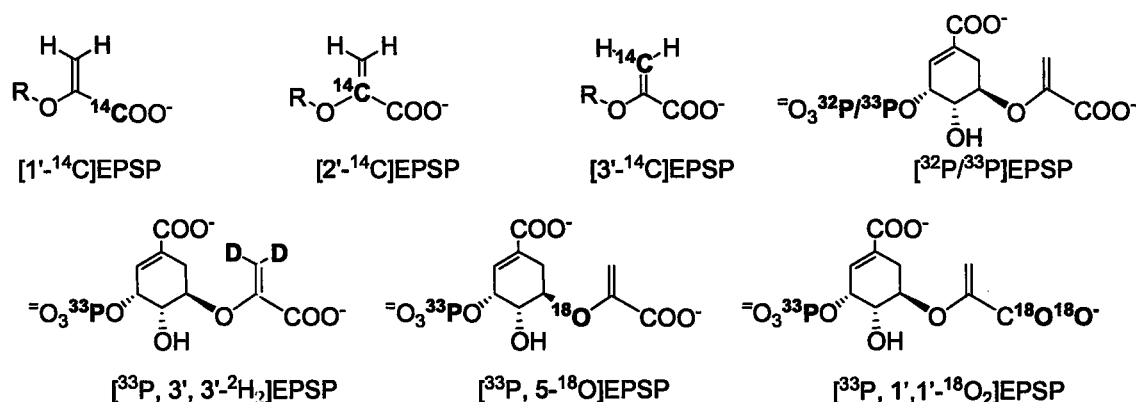


**Figure 15. Radiolabelled EPSPs for KIE measurement.**  $^{32}\text{P}$  and  $^{33}\text{P}$  are remote labels for stable isotopes.

**Table 2. Radiolabelled EPSPs synthesized for KIE measurement**

Name	Concentration (mM)	Radioactivity ( $\mu\text{Ci}$ )	Volume ( $\mu\text{l}$ )	Specific activity ( $\mu\text{Ci}/\mu\text{l}$ )	Isotope abundance
$[1'-^{14}\text{C}]EPSP$	3.5	1.2	150	0.008	
$[2'-^{14}\text{C}]EPSP$	7.0	6.2	130	0.048	
$[3'-^{14}\text{C}]EPSP$	5.3	2.4	150	0.016	
$[^{33}\text{P}]EPSP$	1.1	11.8	120	0.098	
$[^{32}\text{P}]EPSP$	1.0	12.7	100	0.127	
$[^{33}\text{P}, 5-^{18}\text{O}]EPSP$	1.8	3.8	150	0.025	0.55
$[^{33}\text{P}, 1', 1'-^{18}\text{O}_2]EPSP$	2.1	5.7	120	0.048	0.91
$[^{33}\text{P}, 3', 3'-^2\text{H}_2]EPSP$	2.4	2.1	150	0.014	0.97

$^{14}\text{C}$ -labelled EPSPs were synthesized from S3P and labelled pyruvate by coupled reactions of ppsA and AroA. EPSP was purified and quantified by HPLC and the specific activity determined by liquid scintillation counting (Table 2).  $[^{32}\text{P}]$ - and  $[^{33}\text{P}]$ EPSPs were synthesized by coupled AroK and AroA reactions (Table 2).

$[^{33}\text{P}, 1', 1'-^{18}\text{O}_2]EPSP$  was synthesized from  $[^{33}\text{P}]S3P$  and  $[^{18}\text{O}]PEP$ . A parallel reaction was run with  $[^{18}\text{O}]PEP$  but non-radioactive S3P under the same reaction conditions.  $^{18}\text{O}$  enrichment in the non-radioactive sample was determined

by mass spectrometry as a reporter on  $[^{33}\text{P},1',1'-^{18}\text{O}_2]\text{EPSP}$ . Mass spectrometry indicated that 91% of all the oxygen atoms were  $^{18}\text{O}$  labelled (Figure 16).

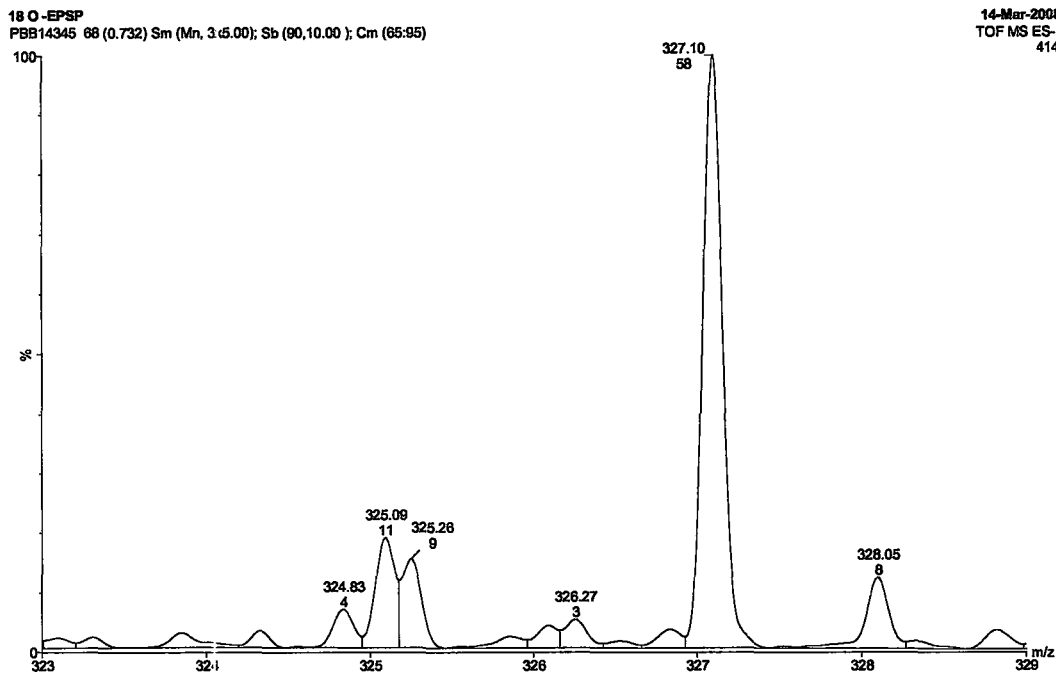


**Figure 16.  $[1',1'-^{18}\text{O}_2]\text{EPSP}$  synthesis.** For unlabelled EPSP in negative mass spectrometry,  $m/z = 323$ . For  $[1',1'-^{18}\text{O}_2]\text{EPSP}$ ,  $m/z = 327$ . 91% of the oxygen atoms at C1' were  $^{18}\text{O}$  labelled.

The synthetic method for  $[^{33}\text{P},5-^{18}\text{O}]\text{EPSP}$  was the same as  $[^{33}\text{P}]\text{EPSP}$  except that  $[5-^{18}\text{O}]\text{shikimic acid}$  was used. A parallel reaction without  $^{33}\text{P}$  was used to measure the extent of  $^{18}\text{O}$  enrichment by mass spectrometry.  $^{18}\text{O}$  enrichment was 55% in  $[5-^{18}\text{O}]\text{EPSP}$  (Figure 17).

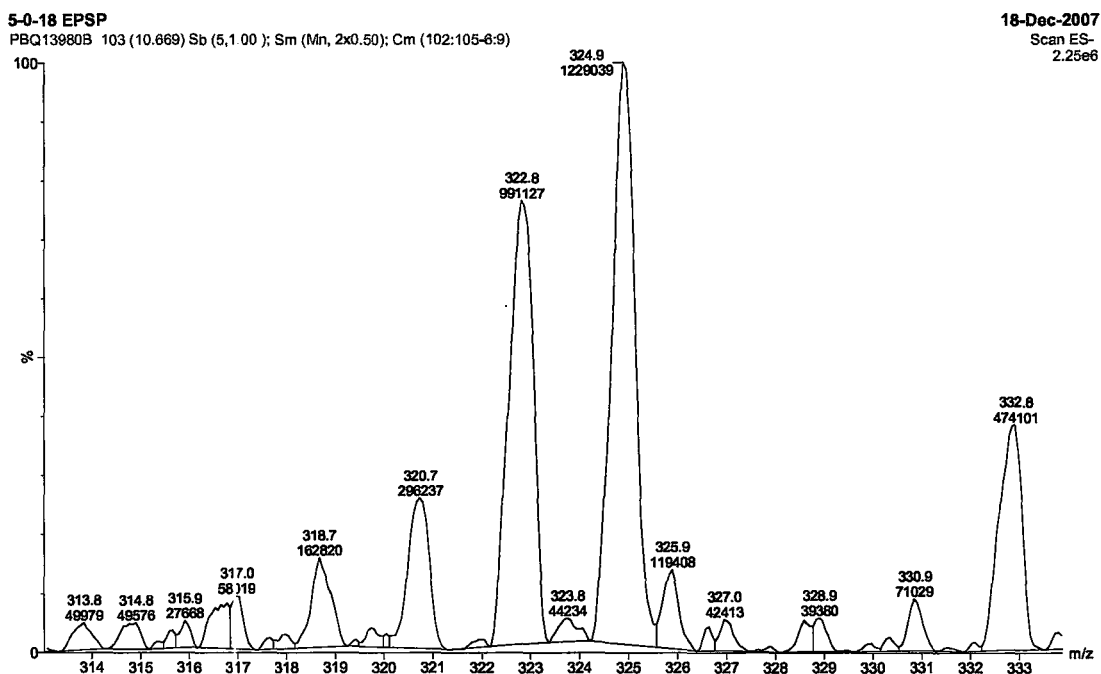


**Figure 17. [5-<sup>18</sup>O]EPSP synthesis.** For unlabelled EPSP in negative mass spectrometry,  $m/z = 323$ . For [5-<sup>18</sup>O]EPSP,  $m/z = 325$ . 55% of EPSP was <sup>18</sup>O labelled.

<sup>2</sup>H-labelled EPSP was synthesized by taking advantage of the fact that the normal AroA reaction is reversible, and hydrogens at position 3' are exchanged with solvent during the reaction. [<sup>33</sup>P]EPSP was incubated with limited Pi in D<sub>2</sub>O to form [<sup>33</sup>P,3',3'-<sup>2</sup>H<sub>2</sub>]EPSP. In a parallel reaction with unlabelled EPSP, the D abundance was determined by mass spectrometry, to be 97% (Figure 18).

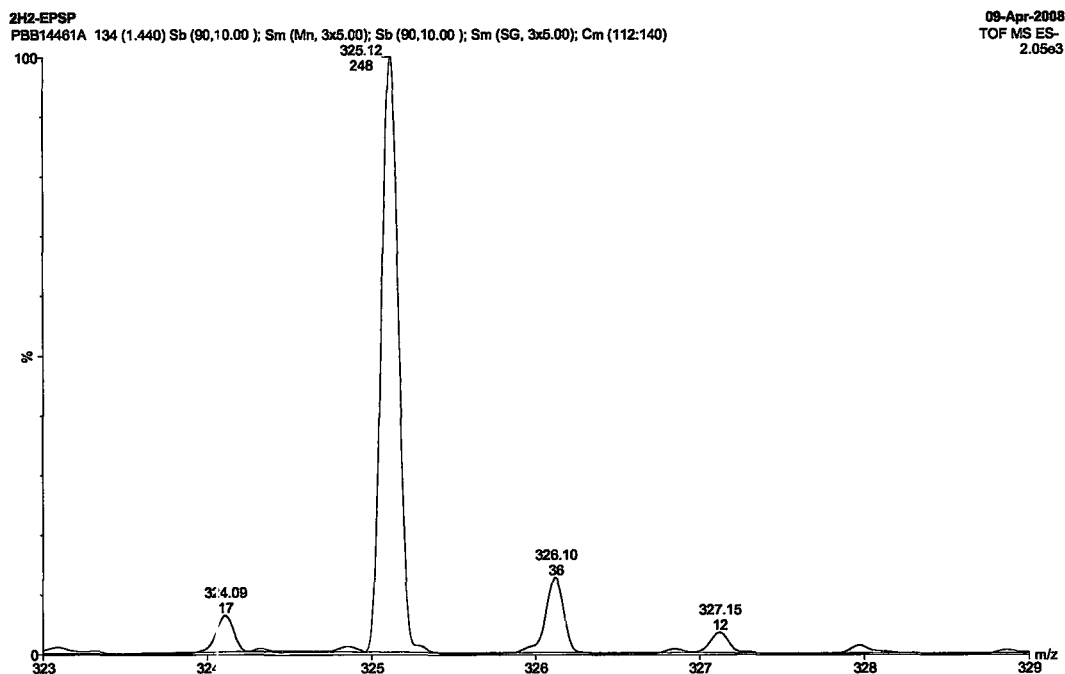


**Figure 18. [3',3'-<sup>2</sup>H<sub>2</sub>]EPSP synthesis.** For unlabelled EPSP in negative mass spectrometry, m/z = 323. For [3',3'-<sup>2</sup>H<sub>2</sub>]EPSP, m/z = 325. 97% of all 3'-H was exchanged to D.

In summary, all the radiolabelled EPSPs were synthesized enzymatically and the abundance of non-radioactive heavy isotopes was determined by mass spectrometry (Table 2).

### Optimization of KIE measurement conditions

The EPSP hydrolysis rate was determined with unlabelled EPSP under the KIE measurement conditions in order to find conditions where the reaction reached 50% completion. With 50  $\mu$ M AroA and 500  $\mu$ M EPSP, it took 50 min at 37 °C. The acid-catalyzed hydrolysis was performed at 90 °C so that 50% completion also took approximately 50 min.

For the <sup>2</sup>H KIE, it was necessary to ensure that there was no Pi present in the solutions in order to avoid <sup>2</sup>H being exchanged with solvent during the normal

reaction to S3P and PEP. A Pi scavenging system was used to remove Pi from all solutions before EPSP and AroA were combined, with [Pi] being monitored with the MG/AM assay (data not shown).

Determining isotope ratios entails counting radioactivity in two “windows”. Window 1 detects decay of the isotope with less energetic  $\beta$ -particles.  $^{14}\text{C}$  and  $^{33}\text{P}$  are detected in Window 1, plus some of the decay of the more energetic isotope,  $^{32}\text{P}$ . Window 2 detects decay of the more energetic isotope,  $^{32}\text{P}$ , only (Figure 10). The energy profiles for  $^{14}\text{C}$ ,  $^{32}\text{P}$ , and  $^{33}\text{P}$  were determined by collecting spectra for 1  $\mu\text{L}$  of each isotope separately (Figure 19). The scintillation counting windows for each isotope pair were determined for future measurement: window 0-650 for  $^{14}\text{C}$ , window 0-700 for  $^{33}\text{P}$  and window 650-1000 or 700-1000 for  $^{32}\text{P}$ .

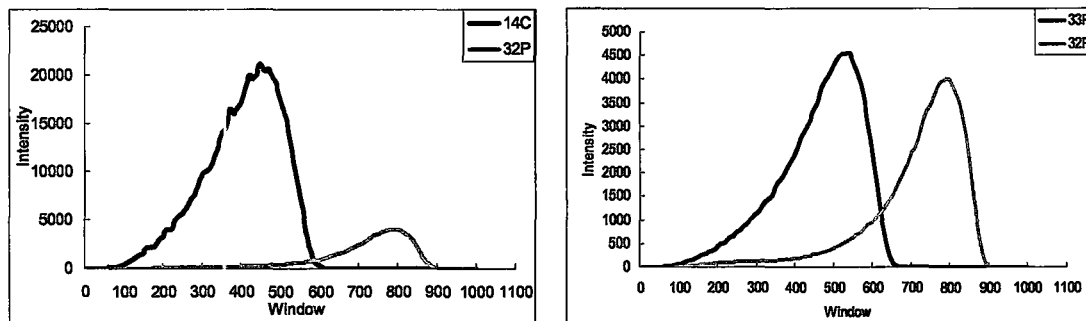


**Figure 19. Energy profiles of  $^{14}\text{C}$  versus  $^{32}\text{P}$  and  $^{33}\text{P}$  versus  $^{32}\text{P}$ .**

Once the reaction of interest is complete, it is important that no further isotope fractionation occurs, as this would lead to artifacts. One possible cause of fractionation is during the separation of the reactants and products. It is known that the isotopic labelling affects chromatographic mobility, which can lead to the isotope ratio being different in the beginning and tailing parts of a peak (47). To

avoid this, it was important to collect the entire peak during separation.

In order to ensure that all radioactivity was accounted for and there were no unexpected reaction products, fractions were collected and counted in the anion exchange chromatography of 0% and 50% reactions containing  $^{14}\text{C}$  and  $^{32}\text{P}$  EPSP (Figure 20). The distributions of  $^{14}\text{C}$  and  $^{32}\text{P}$  in the chromatograms were as expected, showing  $^{14}\text{C}$  in pyruvate, EPSP ketal and EPSP, while  $^{32}\text{P}$  appeared in S3P, EPSP ketal and EPSP. For KIE measurements, pyruvate was collected from 4 to 11 min, S3P from 11 to 16 min, EPSP ketal from 16 to 18 min, and EPSP from 18 to 26 min.

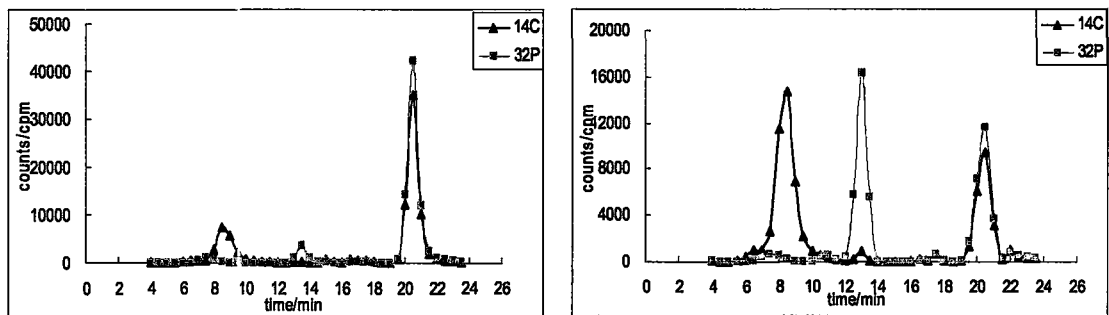


**Figure 20. Radioactivity distribution of EPSP hydrolysis, at 0% (left) and 50% (right) reactions.** Pyruvate: 4-11 min; S3P:11-16 min; EPSP ketal: 16-18 min; EPSP: 18-26 min.

In order to confirm that HPLC separation did not introduce any isotopic fractionation, isotope ratios were measured before and after HPLC anion exchange purification. The Mono Q column did cause around 10% radioactivity loss for each run, but it would not affect the isotope ratios as long as the entire peak was collected. The change in isotope ratios in EPSP which went through HPLC once or twice, such as  $^{14}\text{C}/^{32}\text{P}$  ratio in this case, was as low as 0.3%,

demonstrating that the conditions were reliable enough for real KIE measurement (Table 3).

**Table 3. Isotope ratios before and after HPLC separation**

$^{14}\text{C}/^{32}\text{P}$	Trial 1	Trial 2
Before HPLC	0.631	0.574
After HPLC	0.634	0.574
Ratio	1.005	1.000
Mean	1.003	

### Remote labels

$^{32}\text{P}$  and  $^{33}\text{P}$  were used as remote labels for other non-radioactive isotopes in KIE measurements. A significant KIE at this position is highly unlikely, but to test that, the  $^{32}\text{P}/^{33}\text{P}$  KIE was measured for the AroA-catalyzed reaction.

To measure the  $^{32}\text{P}/^{33}\text{P}$  KIE, 500  $\mu\text{M}$  EPSP containing 0.25  $\mu\text{Ci}$  of each of [ $^{32}\text{P}$ ]- and [ $^{33}\text{P}$ ]EPSP was re-purified and reacted with 50  $\mu\text{M}$  AroA after incubation of both solutions with the Pi scavenging system. The reaction was quenched at 0% and 50% completion, and both reaction mixtures were applied to the Mono Q column. All the peaks were collected and counted to determine the extent of the reaction ( $f$ ) and the KIE using equation 11. The observed KIE was unity (Table 4), as expected, which demonstrated that  $^{32}\text{P}$  and  $^{33}\text{P}$  are appropriate remote labels that do not contribute isotope effects themselves.

**Table 4.  $^{32}\text{P}/^{33}\text{P}$  KIE for AroA-catalyzed EPSP hydrolysis**

Sample #	Extent of reaction	KIE
1	0.509	0.997
2	0.613	1.002
3	0.587	1.002
Average <sup>a</sup>		1.000 ± 0.004

<sup>a</sup> Average of 3 independent trials ± 95% confidence interval.

### **KIEs from AroA-catalyzed EPSP hydrolysis**

KIEs for AroA-catalyzed EPSP hydrolysis were measured as described above. After HPLC separation of the reaction products, the radioactivity in pyruvate, S3P, EPSP ketal and EPSP peaks was determined by scintillation counting and used to calculate KIEs using equation 11 (Table 5 to 10, Figure 21).

**Table 5. [1'- $^{14}\text{C}$ ]EPSP KIE for AroA-catalyzed hydrolysis**

Sample #	Extent of reaction	KIE
1	0.555	1.003
2	0.460	1.007
3	0.715	1.005
Average <sup>a</sup>		1.005 ± 0.002

<sup>a</sup> Average of 3 independent trials ± 95% confidence interval.

**Table 6. [2'- $^{14}\text{C}$ ]EPSP KIE for AroA-catalyzed hydrolysis**

Sample #	Extent of reaction	KIE
1	0.813	1.008
2	0.405	1.014
3	0.565	1.008
Average <sup>a</sup>		1.010 ± 0.003

<sup>a</sup> Average of 3 independent trials ± 95% confidence interval.

**Table 7. [3'-<sup>14</sup>C]EPSP KIE for AroA-catalyzed hydrolysis**

Sample #	Extent of reaction	KIE
1	0.349	1.029
2	0.585	1.030
3	0.348	1.036
Average <sup>a</sup>		1.032 ± 0.005

<sup>a</sup> Average of 3 independent trials ± 95% confidence interval.

**Table 8. [3',3'-<sup>2</sup>H<sub>2</sub>]EPSP KIE for AroA-catalyzed hydrolysis**

Sample #	Extent of reaction	KIE	<sup>2</sup> H enrichment <sup>a</sup>	Corrected KIE <sup>b</sup>
1	0.495	0.989	0.99	0.989
2	0.845	0.990	0.99	0.989
3	0.713	0.990	0.99	0.990
Average <sup>c</sup>				0.990 ± 0.001

<sup>a</sup> Abundance of <sup>2</sup>H in the synthesized EPSP;

<sup>b</sup> Corrected KIE takes the enrichment of isotope into consideration. Corrected KIE = 1-(1-KIE<sub>apparent</sub>)/<sup>2</sup>H enrichment;

<sup>c</sup> Average of 3 independent trials ± 95% confidence interval.

**Table 9. [5-<sup>18</sup>O]EPSP KIE for AroA-catalyzed hydrolysis**

Sample #	Extent of reaction	KIE	<sup>18</sup> O enrichment <sup>a</sup>	Corrected KIE <sup>b</sup>
1	0.716	1.000	0.55	1.000
2	0.458	0.986	0.55	0.975
3	0.809	0.991	0.55	0.984
Average <sup>c</sup>				0.986 ± 0.008

<sup>a</sup> Abundance of <sup>18</sup>O in the synthesized EPSP;

<sup>b</sup> Corrected KIE takes the enrichment of isotope into consideration. Corrected KIE = 1-(1-KIE<sub>apparent</sub>)/<sup>18</sup>O enrichment;

<sup>c</sup> Average of 3 independent trials ± 95% confidence interval.

**Table 10. [1',1'-<sup>18</sup>O<sub>2</sub>]EPSP KIE for AroA-catalyzed hydrolysis**

Sample #	Extent of reaction	KIE	<sup>18</sup> O enrichment <sup>a</sup>	Corrected KIE <sup>b</sup>
1	0.617	0.977	0.91	0.975
2	0.652	0.986	0.91	0.985
3	0.415	0.981	0.83	0.977
Average <sup>c</sup>				0.979 ± 0.006

<sup>a</sup> Abundance of <sup>18</sup>O in the synthesized EPSP;

<sup>b</sup> Corrected KIE takes the enrichment of isotope into consideration. Corrected KIE =  $1 - (1 - \text{KIE}_{\text{apparent}}) / {}^{18}\text{O}$  enrichment;

<sup>c</sup> Average of 3 independent trials  $\pm$  95% confidence interval.

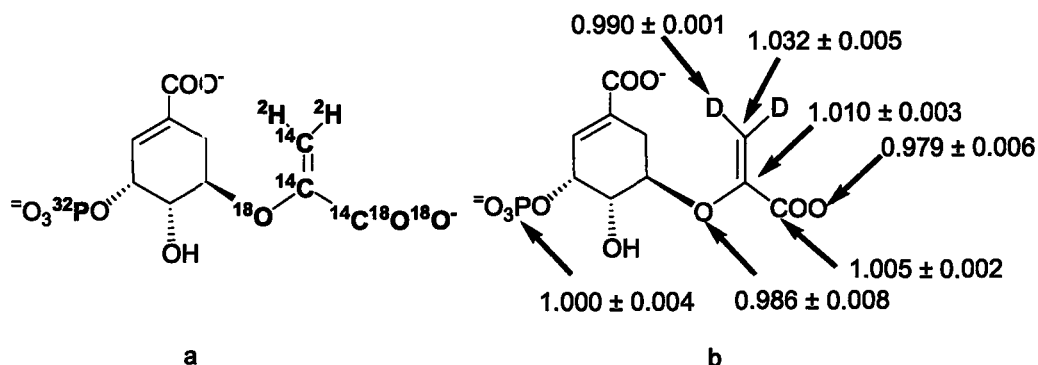


**Figure 21. Summary of KIEs for AroA-catalyzed EPEP hydrolysis.** a). Isotopically labelled EPSPs; b). Experimental KIEs. The average of 3 independent trials  $\pm$  95% confidence interval is reported.

The KIE data from AroA-catalyzed hydrolysis are consistent with a cationic transition state structure (see Discussion). A more accurate and quantitative analysis will require computational simulation, during which a proposed model for TS structure will be set up and all the bond lengths and angles can be determined. KIEs will be calculated and compared with the experimental values above. The computational TS structure that gives the best match of calculated and experimental KIEs is the experimental TS.

### KIEs from acid-catalyzed EPSP hydrolysis

KIEs for acid-catalyzed EPSP hydrolysis were determined using essentially the same method. The one difference was that after labelled EPSP was re-purified as for the AroA-catalyzed reaction, it was not lyophilized because the combination of lyophilization and TBAS from the chromatography buffer caused a side reaction

that consumed EPSP faster than acid-catalyzed hydrolysis. Instead, the chromatographic fraction containing EPSP was adjusted to pH 5.40 and the reaction was started by heating at 90 °C. The rest of the method was the same as for the AroA reaction, and KIEs were calculated in the same way (Table 11 to 16, Figure 22).

**Table 11. [1'-<sup>14</sup>C]EPSP KIE for acid-catalyzed hydrolysis**

Sample #	Extent of reaction	KIE
1	0.594	1.001
2	0.624	1.010
3	0.608	1.011
4	0.582	1.018
Average <sup>a</sup>		1.010 ± 0.007

<sup>a</sup> Average of 4 independent trials ± 95% confidence interval.

**Table 12. [2'-<sup>14</sup>C]EPSP KIE for acid-catalyzed hydrolysis**

Sample #	Extent of reaction	KIE
1	0.645	1.001
2	0.579	1.006
3	0.653	1.002
Average <sup>a</sup>		1.003 ± 0.003

<sup>a</sup> Average of 3 independent trials ± 95% confidence interval.

**Table 13. [3'-<sup>14</sup>C]EPSP KIE for acid-catalyzed hydrolysis**

Sample #	Extent of reaction	KIE
1	0.626	1.003
2	0.612	1.005
3	0.580	1.014
4	0.546	1.012
Average <sup>a</sup>		1.009 ± 0.005

<sup>a</sup> Average of 4 independent trials ± 95% confidence interval.

**Table 14 [3',3'-<sup>2</sup>H<sub>2</sub>]EPSP KIE for acid-catalyzed hydrolysis**

Sample #	Extent of reaction	KIE	<sup>2</sup> H enrichment <sup>a</sup>	Corrected KIE <sup>b</sup>
1	0.633	1.008	0.97	1.008
2	0.674	1.007	0.97	1.007
3	0.610	0.990	0.97	0.990
4	0.585	1.015	0.83	1.018
5	0.672	0.989	0.83	0.987
6	0.919	1.001	0.83	1.001
Average <sup>c</sup>				1.002 ± 0.010

<sup>a</sup> Abundance of <sup>2</sup>H in the synthesized EPSP;

<sup>b</sup> Corrected KIE takes the enrichment of isotope into consideration. Corrected KIE = 1-(1-KIE<sub>apparent</sub>)/<sup>2</sup>H enrichment;

<sup>c</sup> Average of 6 independent trials ± 95% confidence interval.

**Table 15. [5-<sup>18</sup>O]EPSP KIE for acid-catalyzed hydrolysis**

Sample #	Extent of reaction	KIE	<sup>18</sup> O enrichment <sup>a</sup>	Corrected KIE <sup>b</sup>
1	0.679	0.974	0.55	0.954
2	0.693	0.990	0.55	0.981
3	0.652	0.958	0.55	0.924
4	0.674	0.983	0.55	0.970
5	0.668	0.988	0.55	0.978
6	0.635	1.009	0.55	1.016
7	0.679	1.000	0.55	1.000
8	0.575	0.990	0.55	0.981
9	0.63	0.982	0.55	0.968
10	0.612	1.004	0.55	1.008
Average <sup>c</sup>				0.978 ± 0.009

<sup>a</sup> Abundance of <sup>18</sup>O in the synthesized EPSP;

<sup>b</sup> Corrected KIE takes the enrichment of isotope into consideration. Corrected KIE = 1-(1-KIE<sub>apparent</sub>)/<sup>18</sup>O enrichment;

<sup>c</sup> Average of 10 independent trials ± 95% confidence interval.

**Table 16. [1',1'-<sup>18</sup>O<sub>2</sub>]EPSP KIE for acid-catalyzed hydrolysis**

Sample #	Extent of reaction	KIE	<sup>18</sup> O enrichment <sup>a</sup>	Corrected KIE <sup>b</sup>
1	0.609	0.998	0.86	0.998
2	0.681	1.005	0.86	1.006
3	0.635	1.000	0.86	1.000
4	0.657	1.005	0.86	1.006
5	0.808	0.998	0.86	0.998
Average <sup>c</sup>				1.001 ± 0.004

<sup>a</sup> Abundance of <sup>18</sup>O in the synthesized EPSP;

<sup>b</sup> Corrected KIE takes the enrichment of isotope into consideration. Corrected KIE =  $1 - (1 - \text{KIE}_{\text{apparent}}) / ^{18}\text{O}$  enrichment;

<sup>c</sup> Average of 5 independent trials ± 95% confidence interval.

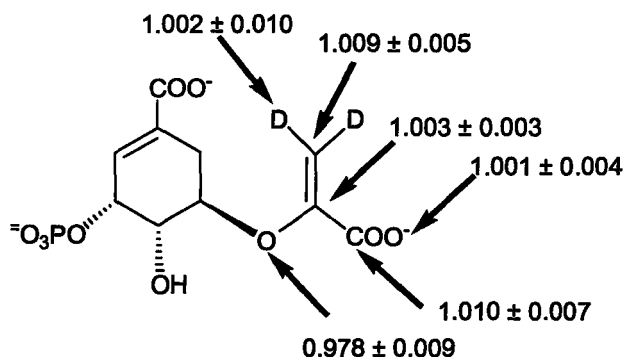


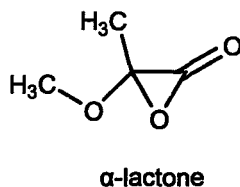
**Figure 22. KIEs for acid-catalyzed EPEP hydrolysis.** The average ± 95% confidence interval is reported.

There was greater variability in the KIEs in the acid-catalyzed reaction, as reflected in the larger 95% confidence interval. Therefore more independent trials were conducted for the acid-catalyzed reactions. The reason for this is not clear. KIEs from acid-catalyzed hydrolysis were not the same as AroA-catalyzed hydrolysis, which implies differences in the transition states and distinct catalytic mechanisms between these two reactions. KIE data from the acid-catalyzed reaction will also be analyzed by computational chemistry as the AroA reaction. A mechanistic comparison between AroA- and acid-catalyzed hydrolysis will then be

made.

### Computational TS structures and their corresponding EIE/KIE

As indicated in the Methods section, the oxacarbenium ion is not stable when optimized by electronic structure methods. An  $\alpha$ -lactone structure was formed after one of the carboxylate oxygens attacked the cationic centre. As a result, a variety of small molecules and computational approaches were tested. This included using continuum solvation, and/or adding water molecules to moderate the reactivity of the cationic center. In addition,  $\text{Li}^+$  or a guanidinium ion was added to interact with and stabilize the carboxylate, decreasing its nucleophilicity.



Optimized structures were found for the *eno*/pyruvyl model, the transition state for C3' protonation, and the oxacarbenium ion product whenever possible. EIEs calculated for the oxacarbenium ion formation should be reasonable estimates of secondary KIEs where little reaction coordinate motion is involved.

One TS structure that was found involves one guanidinium ion and three  $\text{H}_2\text{O}$  molecules (Figure 23). KIEs were calculated for this structure. Water molecules were used to accept and transfer the proton from C3' so that it will not attack the carboxylate group. The guanidinium ion imitates Arg386 residue in the

AroA's active site. The guanidinium nitrogens of Arg386 are located 2.8 Å and 2.9 Å from the carboxylate oxygens of the THI in the AroA(D313A) • THI structure (25), and in a similar orientation to the model structure in Figure 23. They are hypothesized to stabilize the carboxylate group and prevent it from attacking the anomeric carbon.

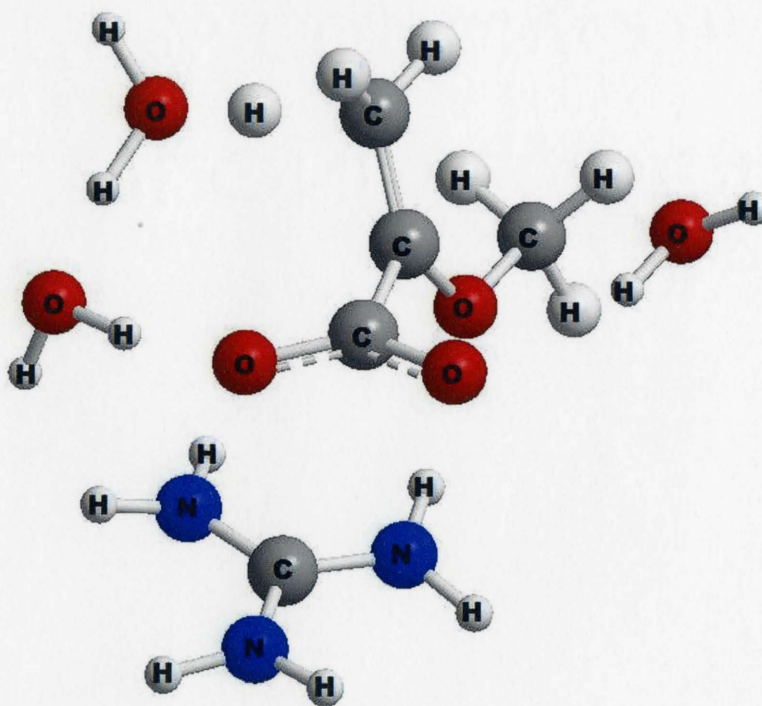


**Figure 23. TS model with one guanidinium ion and three water molecules.** One proton is being stretched away from C3' and transferred to H<sub>2</sub>O nearby. This structure corresponds to the highest energy point in transferring the proton from the hydronium ion to C3'. Blue: nitrogen; grey: carbon; red: oxygen; white: hydrogen.

In the transition state, the C3'-H bond length is 1.450 Å with a bond order of 0.3.<sup>2</sup> The O-H distance is 1.187 Å with a bond order of 0.55. The third H<sub>2</sub>O

<sup>2</sup> Bond order:  $n_{ij} = e^{(r_1 - r_{ij})/0.3}$ , where  $r_{ij}$  is the distance between atoms  $i$  and  $j$  and  $r_1$  is the single bond length between  $i$  and  $j$ .

molecule was placed behind the oxacarbenium ion to stabilize it. The guanidinium ion was located right in front of the carboxylate group to keep the oxygen atoms in place (This TS structure was solved by my supervisor, Dr. Paul Berti).

The fractionation factors ( $Q$ ) for the cationic intermediate, reactant and TS were calculated using *QUIVER*, of which the first two were used to determine EIEs while the latter two were for KIEs. The isotope effects were calculated at 310 K for the AroA reaction (Table 17), and 363 K for the acid-catalyzed reaction (Table 18).

**Table 17. Calculated EIEs/KIEs for AroA-catalyzed hydrolysis at 310 K**

Positions	EIEs	KIEs	Experimental KIEs
1'- <sup>14</sup> C	0.999	1.005	1.005 ± 0.002
2'- <sup>14</sup> C	0.993	0.997	1.010 ± 0.003
3'- <sup>14</sup> C	1.000	1.021	1.032 ± 0.005
5- <sup>18</sup> O	0.991	1.006	0.986 ± 0.008
1',1'- <sup>18</sup> O	1.002	1.030	0.979 ± 0.006
3',3'- <sup>2</sup> H <sub>2</sub>	0.909	0.996	0.990 ± 0.001

**Table 18. Calculated EIEs/KIEs for acid-catalyzed hydrolysis at 363 K**

Positions	EIEs	KIEs	Experimental KIEs
1'- <sup>14</sup> C	0.998	1.006	1.010 ± 0.007
2'- <sup>14</sup> C	0.995	0.999	1.003 ± 0.003
3'- <sup>14</sup> C	1.000	1.021	1.009 ± 0.005
5- <sup>18</sup> O	0.993	1.006	0.978 ± 0.009
1',1'- <sup>18</sup> O	1.001	1.030	1.001 ± 0.004
3',3'- <sup>2</sup> H <sub>2</sub>	0.925	1.006	1.002 ± 0.010

## Discussion

### **Kinetically significant steps**

It is important to know which steps of the reaction the KIEs reflect when performing TS analysis. The non-competitive SDKIEs report on  $k_{cat}$ , the rate-limiting step of the reaction, i.e. the step with the largest activation energy (40). The remaining KIEs were competitive; they report on the second-order rate constant,  $k_{cat}/K_m$ , and reflect the first irreversible step of the reaction. This corresponds to the point with the highest overall energy in the reaction coordinate (40). For acid-catalyzed hydrolysis, the rate-limiting step is also the first irreversible step (Figure 24a); however, this is not always the case for enzymatic reactions (Figure 24b). For AroA- (31) and acid-catalyzed (Joan Lowe-Ching, personal communication) EPSP hydrolysis, it has been determined that the protonation of C3', i.e. the formation of EPSP cation, is the first irreversible step (Figure 24c).

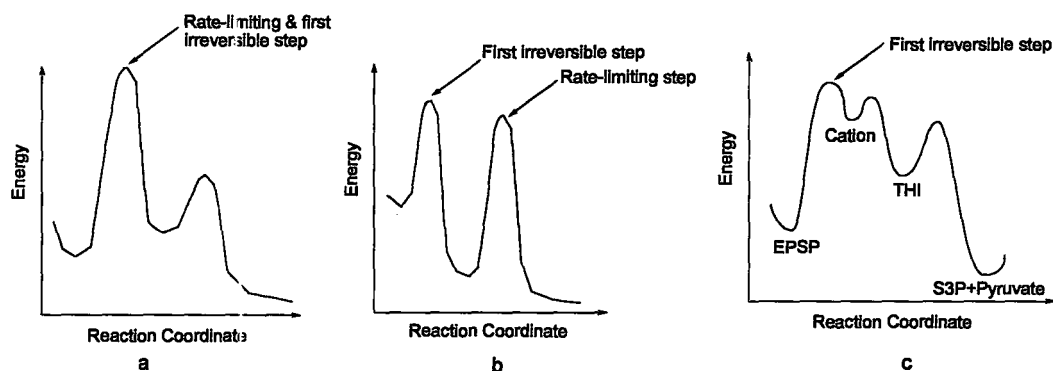


**Figure 24. Kinetically significant steps in the reaction coordinate. a). Rate-limiting step as well as the first irreversible step; b). Rate-limiting step and first irreversible step are separate; c). The formation of EPSP cation acts as the first irreversible step of EPSP hydrolysis.**

### **SDKIE from AroA-catalyzed EPSP hydrolysis**

SDKIEs can tell us whether there is a solvent-based hydron being transferred at the transition state. If a hydron (L) is in flight at the TS of the rate-limiting step, the reaction coordinate motion of the transferring L from solvent will make a large normal contribution to the SDKIE.

The SDKIE for acid-catalyzed EPSP hydrolysis at pH 2.0 and 52 °C was  $2.9 \pm 0.8$  (Joan Lowe-Ching, personal communication). This indicates that a hydron is in flight at the TS, and it is consistent with the conventional mechanism of vinyl ether group hydrolysis, which involves a rate-limiting proton transfer from solvent to C3', followed by rapid attack to the oxacarbenium intermediate by H<sub>2</sub>O (48).

The SDKIE for AroA-catalyzed EPSP hydrolysis was  $0.97 \pm 0.04$ . Although SDKIEs indicate proton transfer in non-enzymatic reactions, they are often complicated in enzymatic reactions by issues like viscosity and solvent D partitioning among the hundreds of amino acids in an enzyme with exchangeable hydrons. Therefore, the information provided by SDKIE is not conclusive. We can only make preliminary interpretation and require more KIE data to support our prediction.

### **Method development**

A protocol for measuring KIEs of AroA- and acid-catalyzed hydrolysis was developed. The KIEs were measured by determining the change in isotope ratios

in EPSP between 0% reaction and partial, 50% reaction. The partial reactions were stopped at around 50% because this is the extent of reaction that gives the lowest error of KIE measurement. The error is a function of errors in determining the extent of the reaction  $f$  and the isotope ratios (49,50). The compromise between these two factors gives rise to the 50% extent reaction.

KIE measurement for acid hydrolysis was similar to the enzymatic one with slight difference (Ayesha Malik, personal communication). The acid reaction was run at 90 °C, pH 5.40 to reach a reasonable reaction rate (27). The re-purified EPSP was injected onto HPLC directly without lyophilization, since the lyophilized TBAS seemed to impact the hydrolysis rate for an unknown reason.

The  $^{32}\text{P}/^{33}\text{P}$  KIE of unity, not only demonstrated that  $[^{32}\text{P}]$  and  $[^{33}\text{P}]$  are valid remote labels without causing any isotope effects themselves, but also indicated that the conditions are reliable enough for KIE measurement.

### **Interpretation of KIEs from AroA-catalyzed EPSP hydrolysis**

AroA-catalyzed EPSP hydrolysis proceeds via the protonation at C3', which is known to be the first irreversible step, and the nucleophilic attack from  $\text{H}_2\text{O}$  on C2'. The possible mechanisms are classified using a More O'Farrell – Jencks reaction diagram (Figure 25). The top left is a stepwise  $A_{\text{H}}^*A_{\text{N}}$  addition where C3' is first protonated (the hydrogen addition step,  $A_{\text{H}}$ ) before the EPSP cation undergoes nucleophilic addition (the  $A_{\text{N}}$  step) by  $\text{H}_2\text{O}$ . The asterisk indicates that protonation and nucleophilic addition occur in separate steps (51).

The diagonal mechanism,  $A_H A_N$ , is concerted protonation and nucleophilic attack. The bottom right mechanism,  $A_N^* A_H$ , involves nucleophilic attack followed by C3' protonation, and is effectively impossible (27). KIE measurement was conducted to distinguish from pure  $A_H^* A_N$ , pure  $A_H A_N$  or somewhere in the continuum between the two extremes

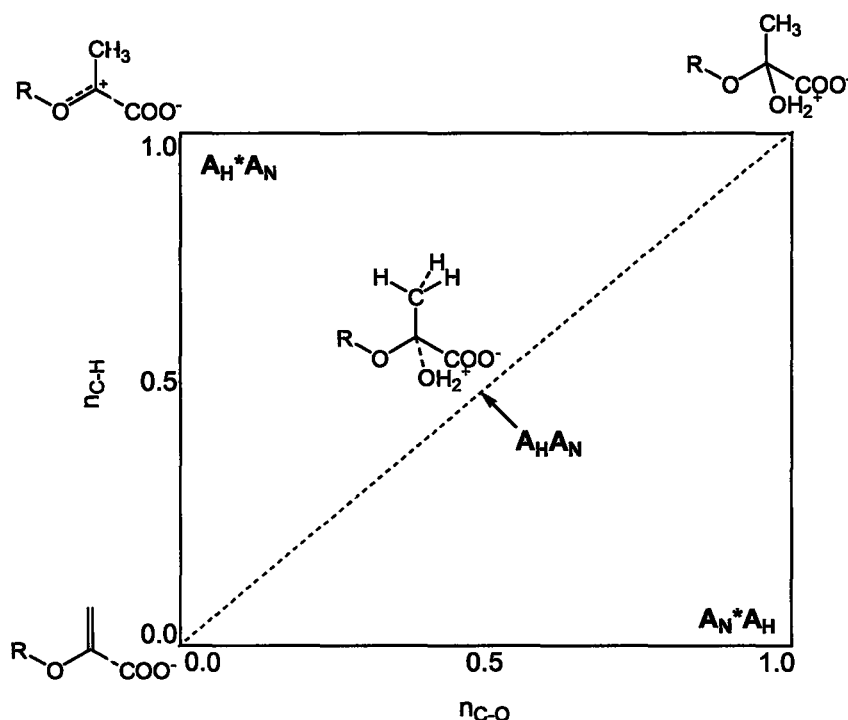
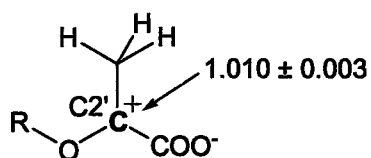
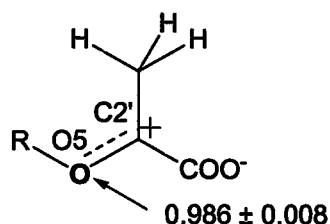


**Figure 25. Reaction diagram for possible mechanisms of addition steps of EPSP hydrolysis.**  $A_H$ : addition of proton;  $A_N$ : addition of nucleophile;  $n_{C-H}$ : C-H bond order;  $n_{C-O}$ : C-O bond order.

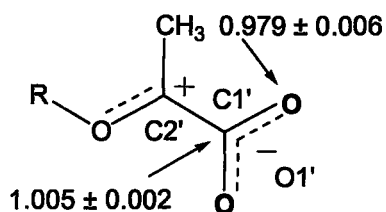
Altogether seven KIEs have been obtained for AroA-catalyzed hydrolysis, including the  $^{32}P/^{33}P$  KIE of unity, which showed that they are valid remote labels for non-radioactive isotopes. The other six will contribute to TS structure prediction and catalytic mechanism analysis. They are all consistent with the formation of EPSP cation or a cationic transition state structure.



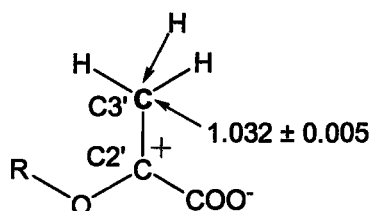
The [2'-<sup>14</sup>C]EPSP KIE is a primary KIE since the C2' atom is involved in bond making and breaking. A normal KIE of  $1.010 \pm 0.003$  indicates a looser vibrational environment between the reactant and the TS. This value is consistent with the predicted cationic transition state structure, with C3' almost fully protonated. C2' has lost bond order to C3' as the C2'-C3'  $\pi$ -bond breaks, which is partly compensated by the increased C2'-O5  $\pi$ -bonding. Since the C2'-C3'  $\pi$ -bond is almost totally broken, the contribution of reaction coordinate motion is small, resulting in a small, normal KIE. It predicts a late TS, approaching the oxacarbenium ion.



An inverse KIE of [5-<sup>18</sup>O]EPSP,  $0.986 \pm 0.008$ , indicates a tighter vibrational environment around O5. This is explained by a shortening of C2'-O5 bond due to the increased  $\pi$ -bonding in the oxacarbenium ion. There is a shift of a lone pair of electrons from O5 towards C2' to contribute to the stabilization of the positively charged C2' in the TS. Therefore there is partial double bond character between C2' and O5, thus resulting in a tighter vibrational environment.

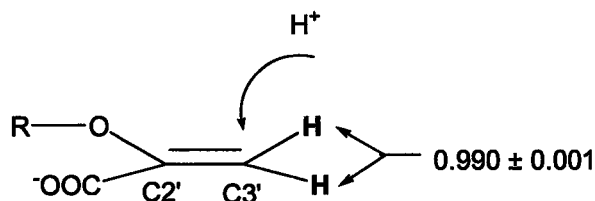


The carboxylate group has a small normal KIE for C1',  $1.005 \pm 0.002$  and an inverse KIE for the two labelled oxygens at O1',  $0.979 \pm 0.006$ . They are also consistent with the formation of a cationic TS. The inverse KIE of O1' shows that the oxacarbenium ion draws the negatively-charged oxygens towards C2' by electrostatic interaction, thus opening the OCO bond angle and giving the carboxylate group partial CO<sub>2</sub> character. The extra attraction from the oxacarbenium ion results in a tighter vibrational environment for O1'. Likewise, the looser C1' environment can be accounted for the electron donation from carboxylate oxygens. Moreover, there was  $\pi$ -conjugation between C2'-C3' double bond and C1'-O1' double bond in EPSP. The breakage of C2'-C3'  $\pi$ -bond in the TS destroys this conjugation and releases the constraint around C1'. Thus the C1'-C2' bond length is getting larger, making a normal contribution to the C1' KIE.



C3' has a large normal KIE,  $1.032 \pm 0.005$ , reflecting a looser vibrational environment. C3' protonation involves it re-hybridizing from  $sp^2$  to  $sp^3$ . Breaking of the C2'-C3'  $\pi$ -bond provides C3' with more vibrational freedom. In addition, a

proton is attacking C3', making a large normal contribution to the KIE due to the reaction coordinate motion.



[3',3'-<sup>2</sup>H<sub>2</sub>]EPSP has an inverse KIE of  $0.990 \pm 0.001$  resulting from a tighter vibrational environment at the TS. Approach of a proton at C3' introduces more steric hindrance at H3', due to a decrease in its out-of-plane vibrational freedom. Meanwhile the reaction coordinate motion makes a normal contribution to the KIE and cancels the effect of steric hindrance to a certain degree, resulting in a small inverse net KIE.

The experimental KIEs are all consistent with a cationic transition state structure. A more accurate and quantitative analysis will require computational simulation, in which a proposed model for TS structure will be set up and all the bond lengths and angles can be determined. KIEs will be calculated theoretically and compared with the experimental data above.

### Interpretation of KIEs from acid-catalyzed EPSP hydrolysis

KIEs from acid-catalyzed hydrolysis were similar to but not identical to the KIEs for the AroA-catalyzed reactions. This implies a slightly different transition state, though the KIEs are also affected by temperature, decreasing at higher temperatures. As demonstrated previously, acid-catalyzed hydrolysis also

proceeds via the formation of the EPSP cation. Protonation of C3' is the first irreversible step, as it is in the enzymatic reaction. As a result, we propose a transition state with oxacarbenium ion character for acid-catalyzed EPSP hydrolysis as well. However, considering that several KIEs from the acid reaction are close to unity, its transition state might be either earlier than the enzymatic reaction with little proton attack and cationic character (Figure 26a), or much later with C3'-H bond almost fully formed (Figure 26b).

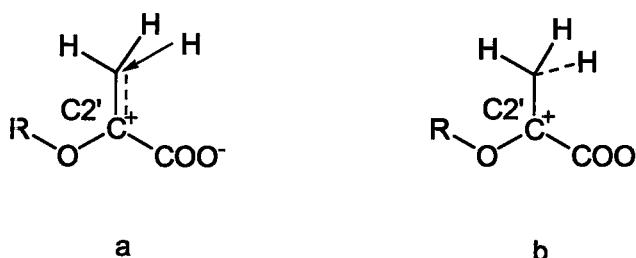
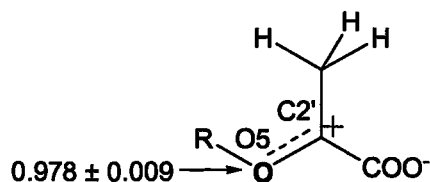
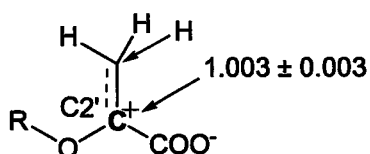


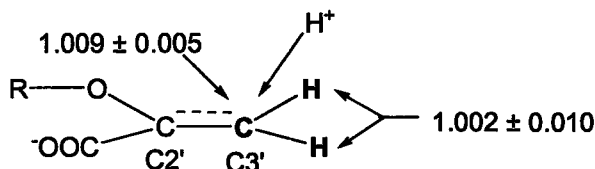
**Figure 26. Proposed TS structures for acid catalyzed hydrolysis.** a). Early TS with proton just starting to attack and little oxacarbenium ion character; b). Late TS with C-H bond almost fully formed; H<sub>2</sub>O may also start to attack C2'.



A more inverse  $5\text{-}^{18}\text{O}$  KIE than the enzymatic reaction,  $0.978 \pm 0.009$ , obviously supports a late TS. It indicates a more constrained vibrational environment around O5, resulting from the donation of O5 lone pair electrons towards C2' to stabilize the oxacarbenium ion. This  $\pi$ -bonding between C2' and O5 increases the C2'-O5 bond order.

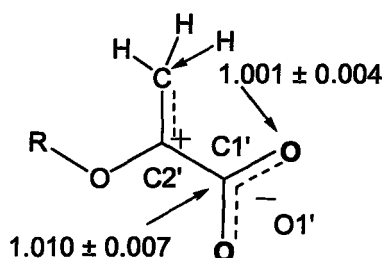


The  $[2'\text{-}^{14}\text{C}]$ EPSP KIE,  $1.003 \pm 0.003$ , is close to unity, which is consistent with the early TS model. In the early TS, the  $\text{C2}'\text{-C3}'$   $\pi$ -bond is breaking, which will lead to the decrease of bond order around  $\text{C2}'$ , making a slightly normal contribution to KIE. On the other hand, if it is a late TS, the breaking  $\text{C2}'\text{-C3}'$   $\pi$ -bond is partially replaced by the formation of  $\text{C2}'\text{-O}$  bond, making a normal but small contribution to KIE. Meanwhile, the attack of  $\text{H}_2\text{O}$  will result in a large reaction coordinate motion. The combination of these two factors should lead to a larger normal KIE.



Both  $[3'\text{-}^{14}\text{C}]$ - and  $[3',3'\text{-}^2\text{H}_2]$ EPSP have KIEs close to unity,  $1.009 \pm 0.005$  and  $1.002 \pm 0.010$  respectively, resulting from a slightly looser vibrational environment. They both support the early TS. When proton starts to attack  $\text{C3}'$  and the  $\text{C2}'\text{-C3}'$   $\pi$ -bond begins to break, they both have a normal but small effect on  $\text{C3}'$  KIE, consistent with the current value. Similarly for the  $[3',3'\text{-}^2\text{H}_2]$ EPSP KIE, when the H is just starting to protonate  $\text{C3}'$ , it will cause a small reaction coordinate motion to  $\text{H3}'$  as well as a little steric hindrance to decrease its out-of-plane vibration. These two effects cancel each other and result in a net KIE

of unity.



Unlike the enzymatic KIE, the carboxylate oxygen for acid reaction is a KIE close to unity,  $1.001 \pm 0.004$ , implying there is little positive charge accumulation at C2' as in the enzymatic reaction. Therefore there is no electrostatic attraction from the oxacarbenium ion and the vibrational environment of O1' does not change significantly. This interpretation matches the prediction of an early TS. C1' has a normal KIE of  $1.010 \pm 0.007$ , due to the decreasing of  $\pi$ -conjugation between C2'-C3' and carboxylate group as the C2'-C3'  $\pi$ -bond is getting weaker. The less constrained vibrational environment around C1' accounts for its normal KIE. It also supports an early TS since in the late TS the incoming H<sub>2</sub>O will bring in more steric hindrance to C1', resulting in an inverse KIE.

There is a contradiction in the interpretation of the 5-<sup>18</sup>O KIE compared to the other labels. The 5-<sup>18</sup>O KIE supports a late TS compared with the enzymatic reaction while all the other positions match better with an early TS. In either case, it employs a slightly different mechanism from the AroA reaction. This is just a qualitative analysis of the KIE data; a more accurate and quantitative analysis is required to explore the transition state structure and catalytic mechanism of acid reaction.

## Computational TS and experimental TS

The first TS model included one guanidinium ion and two H<sub>2</sub>O molecules, plus a hydronium ion that was transferring a proton to C3'. Guanidinium mimicked the Arg386 in the active site of AroA to stabilize the carboxylate group. Two H<sub>2</sub>O molecules helped to stabilize the system as the third one donated a proton to C3'. At the transition state, the C3'-H3' bond was 1.45 Å, while the O-H3' distance was 1.19 Å. Thus, the C3'-H3' bond order was 0.3 and the O-H3' bond order was 0.55, indicating that the proton was roughly half-transferred in the TS structure. KIEs and EIEs were calculated computationally for this TS structure (Figure 27, 28).

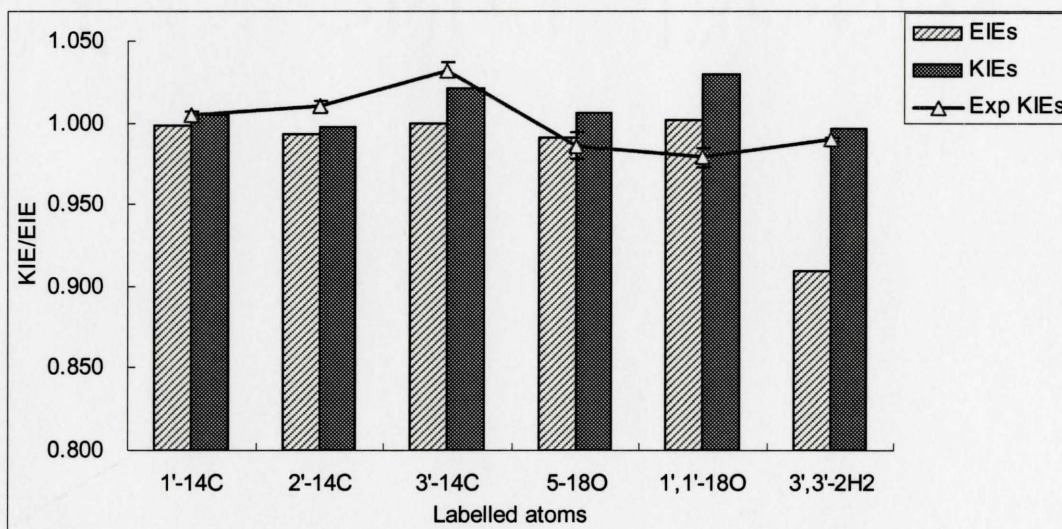


**Figure 27. Comparison of calculated EIEs/KIEs with the experimental KIEs for AroA-catalyzed hydrolysis.** Both calculation and measurement were done at 310 K. Calculated values are shown as bars while experimental values are shown as symbols.

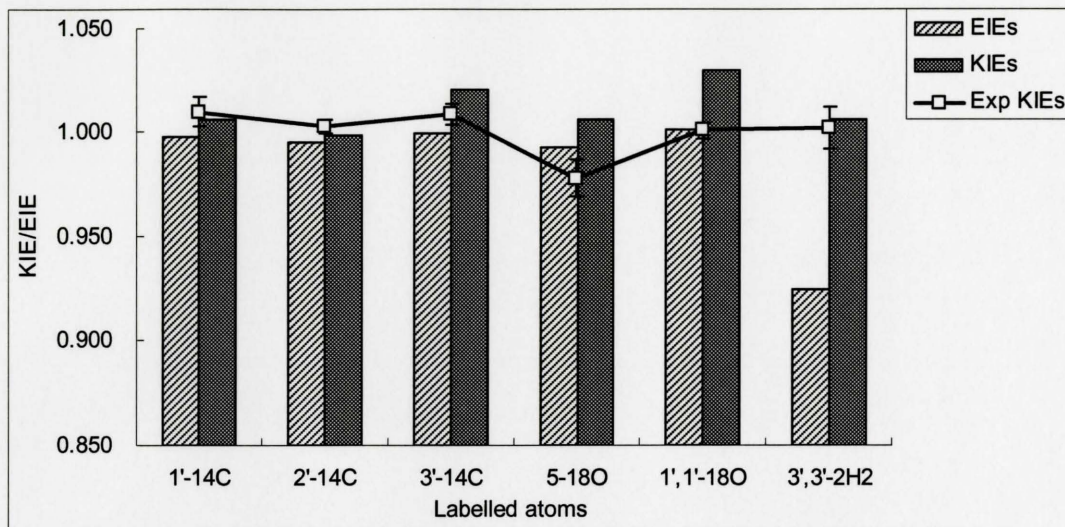


**Figure 28. Comparison of calculated EIEs/KIEs with the experimental KIEs for acid-catalyzed hydrolysis.** Both calculation and measurement were done at 363 K. Calculated values are shown as bars while experimental values are shown as symbols.

The guanidinium TS model worked better for the AroA-catalyzed reaction, since the guanidinium was mimicking the real active site inside the enzyme. Other models, such as lithium with three water molecules failed to give theoretical EIEs/KIEs that match the experimental values, probably because they involved other molecules not existing in AroA or solution environment (data not shown).

Calculated KIEs rather than EIEs match better with experimental KIEs, as expected, especially at the positions of 3'-<sup>14</sup>C and 3',3'-<sup>2</sup>H<sub>2</sub> where the contribution from reaction coordinate motion is obvious. As a result, EIE is a good indicator for secondary KIE only where no bond formation or breaking are occurring. Most of the calculated KIEs have a good agreement with the experimental KIEs, demonstrating that the computational TS structure is similar to the real TS. However, the match of computational to experimental KIEs for 5-<sup>18</sup>O and 1',1'-<sup>18</sup>O

were poor. The discrepancy appears to arise from a large reaction coordinate contribution, given the fact that the calculated EIEs were closer to the real values than the calculated KIEs. This likely represents a limitation of the computational model. With a limited number of solvent molecules, proton transfer is coupled to other molecular motions in the model, where, in reality, the large number of atoms surround the TS would prevent this kind of coupling.

Although the calculated KIEs from the current TS model do not perfectly match the experimental KIEs, it can provide some information. The TS structure from the guanidinium model is consistent with the cationic TS as predicted from the qualitative analysis of KIE values, though the C-H bond formation is not as advanced as might have been expected based on the qualitative interpretation of the KIEs. All the rest bond lengths and bond angles are known from the guanidinium TS structure, which could be a good starting point for designing potent AroA inhibitors.

Similar to the enzymatic reaction, calculated KIEs/EIEs of acid hydrolysis match well with the experimental values except the 5-<sup>18</sup>O and 1',1'-<sup>18</sup>O KIEs. Compared with the acid-catalyzed hydrolysis, the AroA reaction has a slightly better agreement between calculated and experimental KIEs as expected, since the guanidinium TS model was set up resembling the active site of AroA rather than the solution environment. Another model with a self consistent reaction field (SCRF) mimicking the aqueous solvation is being tested, which hopefully can provide a better agreement for the acid reaction.

## **Conclusions and Future Work**

To explore the transition state structure of AroA, a series of radiolabelled EPSPs were synthesized. A KIE measurement method was developed, and KIEs were measured for AroA- and acid-catalyzed hydrolysis. KIEs at six positions around the reaction center were successfully obtained and qualitatively interpreted. KIEs from both reactions support a cationic transition state structure. A TS model with a guanidinium ion was set up computationally and its theoretical KIEs/EIEs were calculated from its structure and vibrational frequency. Calculated KIEs have a good agreement with the experimental values except the 5-<sup>18</sup>O and 1',1'-<sup>18</sup>O KIEs, calling for further computational modification.

Future work includes the improvement of guanidinium TS model so that a better agreement can be achieved. Other models such as TS with SCRF will also be developed and tested to determine the real TS structure, based on which TS-resembling inhibitors of AroA will be synthesized and screened. Those potent inhibitors will have a wide application from herbicides to antimicrobial drugs. After the TS structures for both AroA and acid reactions are solved, it will be possible to compare the catalytic mechanisms they employ, which can provide a more comprehensive understanding of the novel enzyme. Moreover, the method of measuring and analyzing KIEs reactions can be extended to other enzymes, to explore their mechanisms and cast light on potential inhibitor design. One special case in point is MurA, the homologous enzyme of AroA.

## References

1. Duncan, K., and Barry, C. E. (2004) *Curr. Opin. Microbiol.* **7**, 460-465
2. Robertson, J. G. (2005) *Biochemistry* **44**, 5561-5571
3. Nelson, D. L., and Cox, M. M. (2000) *Lehninger Principles of Biochemistry*, Third Edition Ed., Worth Publisher
4. Herrmann, K. M. (1995) *Plant Cell* **7**, 907-919
5. Bentley, R. (1990) *Crit. Rev. Biochem. Mol. Biol.* **25**, 307-384
6. Anderson, K. S., and Johnson, K. A. (1990) *Chem. Rev.* **90**, 1131-1149
7. James A, S., and Gruys, K. J. (1997) *Acc. Chem. Res.* **30**, 2-8
8. Schonbrunn, E., Eschenburg, S., Shuttleworth, W. A., Schloss, J. V., Amrhein, N., Evans, J. N. S., and Kabsch, W. (2001) *Proc. Natl. Acad. Sci. USA* **98**, 1376-1380
9. Lewis, J., Johnson, K. A., and Anderson, K. S. (1999) *Biochemistry* **38**, 7372-7379
10. Zhang, F., and Berti, P. J. (2006) *Biochemistry* **45**, 6027-6037
11. Anton, D. L., Hedstrom, L., Fish, S. M., and Abeles, R. H. (1983) *Biochemistry* **22**, 5903-5908
12. Park, H., Hilsenbeck, J. L., Kim, H. J., Shuttleworth, W. A., Park, Y. H., and Evans, J. N. (2004) *Mol. Microbiol.* **51**, 963-971
13. Gruys, K. J., Walker, M. C., and Sikorski, J. A. (1992) *Biochemistry* **31**, 5534-5544
14. Gruys, K. J., Marzabadi, M. R., Pansegrau, P. D., and Sikorski, J. A. (1993) *Arch. Biochem. Biophys.* **304**, 345-351
15. Barlow, P. N., Appleyard, R. J., Wilson, B. J. O., and Evans, J. N. S. (1989) *Biochemistry* **28**, 7985-7991
16. Zemell, R. I., and Anwar, R. A. (1975) *J. Biol. Chem.* **250**, 4959-4964
17. Jakeman, D. L., Mitchell, D. J., Shuttleworth, W. A., and Evans, J. N. S. (1998) *Biochemistry* **37**, 12012-12019
18. Anderson, K. S. (2005) *Arch. Biochem. Biophys.* **433**, 47-58
19. Byczynski, B., Mizyed, S., and Berti, P. J. (2003) *J. Am. Chem. Soc.* **125**, 12541-12550
20. Anderson, K. S., and Johnson, K. A. (1990) *J. Biol. Chem.* **265**, 5567-5572
21. Marquardt, J. L., Brown, E. D., Walsh, C. T., and Anderson, K. S. (1993) *J.*

- Am. Chem. Soc.* **115**, 10398-10399
22. Asano, Y., Lee, J. J., Shieh, T. L., Spreafico, F., Kowal, C., and Floss, H. G. (1985) *J. Am. Chem. Soc.* **107**, 4314-4320
  23. Kim, D. H., Tucker-Kellogg, G. W., Lees, W. J., and Walsh, C. T. (1996) *Biochemistry* **35**, 5435-5440
  24. An, M., Maitra, U., Neidlein, U., and Bartlett, P. A. (2003) *J. Am. Chem. Soc.* **125**, 12759-12767
  25. Eschenburg, S., Kabsch, W., Healy, M. L., and Schonbrunn, E. (2003) *J. Biol. Chem.* **278**, 49215-49222
  26. Leo, G. C., James A, S., and Sammons, R. D. (1990) *J. Am. Chem. Soc.* **112**, 1653-1654
  27. Clark, M. E., and Berti, P. J. (2007) *Biochemistry* **46**, 1933-1940
  28. Stallings, W. C., Abdel-Meguid, S. S., Lim, L. W., Shieh, H.-S., and Dayringer, H. E. (1991) *Proc. Natl. Acad. Sci. USA* **88**, 5046-5050
  29. Schonbrunn, E., Sack, S., Eschenburg, S., Perrakis, A., Krekel, F., Amrhein, N., and Mandelkow, E. (1996) *Structure* **4**, 1065-1075
  30. Mized, S., Wright, J. E. I., Byczynski, B., and Berti, P. J. (2003) *Biochemistry* **42**, 6986-6995
  31. Clark, M. E. (2006) Understanding the AroA mechanism: Evidence for enolpyruvyl activation and kinetic isotope effect measurement. In. *Biochemistry*, McMaster University
  32. Alberg, D. G., Lauhon, C. T., Nyfeler, R., Fassler, A., and Bartlett, P. A. (1992) *J. Am. Chem. Soc.* **114**, 3535-3546
  33. Alberg, D. G., and Bartlett, P. A. (1989) *J. Am. Chem. Soc.* **111**, 2337-2338
  34. Van Vleet, J. L., Reinhardt, L. A., Miller, B. G., Sievers, A., and Cleland, W. W. (2008) *Biochemistry* **47**, 798-803
  35. Amyes, T. L., and Richard, J. P. (2007) *ACS Chem. Biol.* **2**, 711-714
  36. Lewandowicz, A., and Schramm, V. L. (2004) *Biochemistry* **43**, 1458-1468
  37. Berti, P. J., and McCann, J. A. B. (2006) *Chem. Rev.* **106**, 506-555
  38. Dhekney, G. (2004) Kinetic Isotope Effects on the AroA Reaction: A Mechanistic Investigation of the AroA Reaction. In. *Biochemistry*, McMaster University
  39. Lee, J. K., Bain, A. D., and Berti, P. J. (2004) *J. Am. Chem. Soc.* **126**, 3769-3776
  40. Berti, P. J., and Tanaka, K. S. E. (2002) *Adv. Phys. Org. Chem.* **37**, 239-314

41. McCann, J. A. B. (2006) Study of the MutY and Acid Catalyzed Mechanisms of *N*-Glycoside Hydrolysis. In. *Biochemistry*, McMaster University
42. Jakeman, D. L., and Evans, J. N. S. (1998) *Bioorg. Chem.* **26**, 245-253
43. Pace, C. N., Vajdos, F., Fee, L., Grimsley, G., and Gray, T. (1995) *Protein Sci.* **4**, 2411-2423
44. Anderson, K. S., Sikorski, J. A., and Johnson, K. A. (1988) *Biochemistry* **27**, 1604-1610
45. Veldhoven, P. P. V., and Mannaerts, G. P. (1987) *Anal. Biochem.* **161**, 45-48
46. Saunders, M., Laidig, K. E., and Wolfsberg, M. (1989) *J. Am. Chem. Soc.* **111**, 8989-8994
47. Wade, D. (1999) *Chem. Biol. Interact.* **117**, 191-217
48. Kresge, A. J., Leibovitch, M., and James A, S. (1992) *J. Am. Chem. Soc.* **114**, 2618-2622
49. Singleton, D. A., and Thomas, A. A. (1995) *J. Am. Chem. Soc.* **117**, 9357-9358
50. Duggleby, R. G., and Northrop, D. B. (1989) *Bioorg. Chem.* **17**, 177-193
51. Guthrie, R. D. (1989) *Acc. Chem. Res.* **22**, 343-349